JOURNAL OF GEOPHYSICAL RESEARCH, VOL. 107, NO. D19, 8020, doi:10.1029/2000JD000037, 2002

Aerosol optical properties during INDOEX 1999: Means, variability, and controlling factors

P. K. Quinn,[1,2] D. J. Coffman,[1,2] T. S. Bates,[1,2] T. L. Miller,[1,2] J. E. Johnson,[1,2] E. J. Welton,[3] C. Neusüss,[4] M. Miller,[5] and P. J. Sheridan[6]

Received 13 October 2000; revised 20 March 2001; accepted 3 April 2001; published 6 September 2002.

[1] As part of the Indian Ocean Experiment (INDOEX) 1999 Intensive Field Phase, measurements of aerosol properties were made on board the R/V *Ronald H. Brown* in the Indian Ocean north and south of the Intertropical Convergence Zone (ITCZ) in the Arabian Sea and in the Bay of Bengal. On the basis of air mass trajectories, eight air mass source regions were identified including the southern hemisphere Atlantic; southern hemisphere Indian Ocean; northern hemisphere Indian Ocean; east Indian subcontinent where trajectories came from near Calcutta, through the southern portion of India, and then to the ship; Indian subcontinent where trajectories came from across central India to the ship; Arabia; Arabia/Indian subcontinent, a mixed region where lower-level trajectories came from Arabia and upper-level trajectories came from India; and Arabian Sea/coastal India where trajectories came from along the coast of India to the ship. Properties of the aerosol measured in the marine boundary layer included chemical composition, number size distribution, and scattering and absorption coefficients. In addition, vertical profiles of aerosol backscatter and optical depth were measured. Presented here as a function of air mass source region are the concentrations and mass fractions of the dominant aerosol chemical components, the fraction of the extinction measured at the surface due to each component, mass extinction efficiencies of the individual components, aerosol scattering and absorption coefficients, single scattering albedo, Ångström exponent, and optical depth. All results except aerosol optical depth are reported at the measurement relative humidity of 55 ± 5%. For air masses that originated from the two southern hemisphere marine regions (southern hemisphere Atlantic and Indian Ocean), sea salt dominated the extinction by sub-1 μm and sub-10 μm aerosol particles. The ratios of sub-1μm to sub-10 μm extinction were the lowest measured of all air mass source regions (mean values of 28 and 40%) due to the dominance of the aerosol mass by supermicron sea salt. In addition, aerosol optical depths were the lowest measured averaging 0.06 ± 0.03. Non-sea-salt (nss) sulfate aerosol concentrations in air masses from the northern hemisphere Indian Ocean were a factor of 6 higher than those in southern hemisphere air masses, while submicron sea-salt concentrations were comparable. Sulfate aerosol made up 40% of the sub-1μm extinction, while sea salt dominated the sub-10 μm extinction. Aerosol optical depths for this source region averaged 0.10 ± 0.03. A mean single scattering albedo near 0.89 and detectable black carbon (BC) concentrations (0.14 ± 0.05 μg m^{-3}) indicated the transport of continentally derived aerosol to the ITCZ. The two regions influenced by low-level (500 m) airflow from Arabia had higher concentrations of submicron nss sulfate, particulate organic matter (POM), and inorganic oxidized material (IOM) than were observed in the marine regions. Concentrations of supermicron IOM were comparable to supermicron sea-salt concentrations. Nss sulfate aerosol dominated the sub-1 μm extinction and made significant contributions to the sub-10 μm extinction. Sea salt dominated the supermicron extinction. Mean BC contributions to submicron extinction were 8 and 12%. Single scattering albedo values averaged 0.93 ± 0.02 and 0.89 ± 0.02 for these two source regions. Aerosol optical depths averaged 0.19 ± 0.12 and 0.38 ± 0.07 with the higher value due to upper-level (2500 m) flow from India. Regions influenced by low-level airflow from the Indian subcontinent had the highest submicron nss sulfate, POM, BC, and IOM concentrations measured during the experiment. Supermicron sea-salt concentrations were lower than or comparable to supermicron nitrate concentrations. Sub-1 μm and sub-10

[1]Pacific Marine Environmental Laboratory, NOAA, Seattle, Washington, USA.
[2]Joint Institute for the Study of the Atmosphere and Ocean, University of Washington, Seattle, USA.
[3]Goddard Earth Science and Technology Center, University of Maryland, Baltimore County, Greenbelt, USA.
[4]Institute for Tropospheric Research, Leipzig, Germany.
[5]Environmental Sciences Department, Brookhaven National Laboratory, Upton, New York, USA.
[6]Climate Monitoring and Diagnostics Laboratory, NOAA, Boulder, Colorado, USA.

0148-0227/02/2000JD000037$09.00

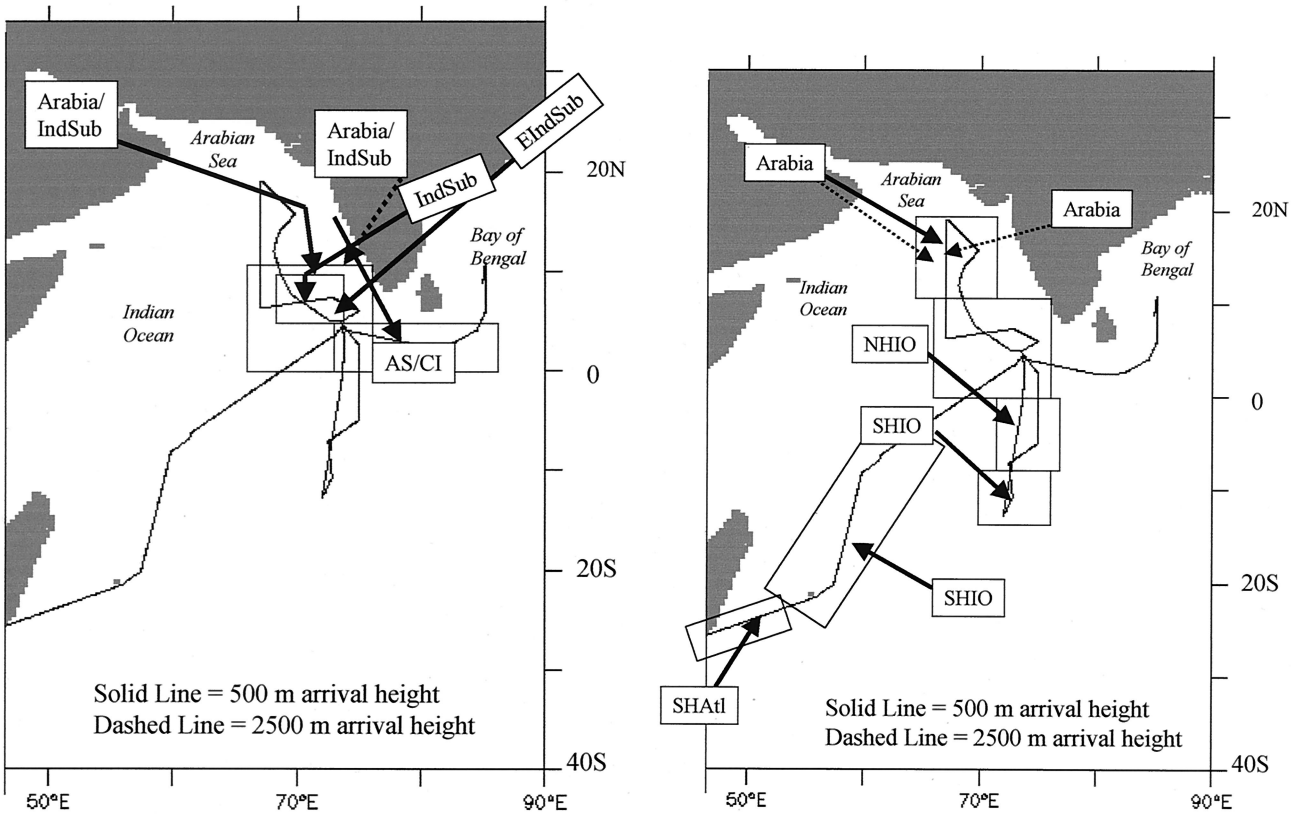

Figure 1. R/V *Ronald H. Brown* cruise track. Boxes indicate where the ship was located along the cruise track when air masses from the different source regions were encountered. Airflow to the ship for each source and geographical region is shown by 500 m arrival height trajectories (solid line). For geographical regions where the 500 m and 2500 m arrival height trajectories were different, airflow based on the 2500 m arrival height trajectories also is shown (dashed line).

μm extinction were dominated by nss sulfate aerosol although a burning component consisting of BC, KNO_3, and K_2SO_4 made a nearly equivalent contribution. These regions had a mean single scattering albedo of 0.85 $\pm$ 0.01, the lowest measured for any region. Mean aerosol optical depths were highest (0.3 to 0.4) for regions with low-level or upper-level airflow from the Indian subcontinent. *INDEX TERMS:* 0305 Atmospheric Composition and Structure: Aerosols and particles (0345, 4801); 1610 Global Change: Atmosphere (0315, 0325); 0365 Atmospheric Composition and Structure: Troposphere--composition and chemistry; *KEYWORDS:* aerosol chemical composition, aerosol mass extinction efficiencies, aerosol mass fractions, aerosol optical depth

Citation: Quinn, P. K., D. J. Coffman, T. S. Bates, T. L. Miller, J. E. Johnson, E. J. Welton, C. Neusüss, M. Miller, and P. J. Sheridan, Aerosol optical properties during INDOEX 1999: Means, variability, and controlling factors, *J. Geophys. Res.*, *107*(D19), 8020, doi:10.1029/2000JD000037, 2002.

1. Introduction

[2] The 1999 Indian Ocean Experiment (INDOEX) Intensive Field Phase (IFP) was conducted in February and March during the winter monsoon season. The study area included the Arabian Sea, the Bay of Bengal, and the Indian Ocean north and south of the Intertropical Convergence Zone (ITCZ) (Figure 1). In this region, during this time of year, continentally derived aerosol chemical components may be transported from the Indian subcontinent and nearby nations to the marine environment where they mix with marine aerosol components. These continental chemical components include soil dust from natural and anthropogenic processes, sulfates and fly ash from industrial processes and fossil fuel combustion, and carbonaceous species from biomass burning, biofuel burning, fossil fuel combustion, and vegetation. The marine chemical components include sea salt and biogenically derived sulfates and carbonaceous species. Hence the region is ideal for assessing the radiative significance of a number of continental and marine aerosol chemical components, one of the major goals of INDOEX.

[3] INDOEX was an international, multiplatform experiment involving two ships, three aircraft, two field stations, satellite observations, and a modeling component. The National Oceanic and Atmospheric Administration (NOAA) Research Vessel *Ronald H. Brown* participated in the 1999 IFP with instrumentation on board capable of characterizing both surface and column aerosol properties (in situ instrumentation

Table 1. Air Mass Regions As a Function of Day of Year During the Experiment[a]

Time Period	Air Mass Region	Abbreviation	Characterization[b]
41–49.5	500 m[c]: SH Atlantic 2500: SH Atlantic	SHAtl	SHmX, SHmT
49.5–56.58 and 78.25–79.5	500 m: SH Indian Ocean 2500: SH Indian Ocean	SHIO	SHmT none
63.56–65.24	500 m: east Indian subcontinent 2500 m: east Indian subcontinent	EIndSub	NHcT
65.24–66.5	500 m: central Indian subcontinent 2500 m: east or central Indian subcontinent	IndSub	NHcT
67–68 and 70.6–76	500 m: Arabia 2500 m: Indian subcontinent	Arabia/IndSub	none NHcX
68–70.42	500 m: Arabia 2500 m: Arabia or Indian subcontinent	Arabia	NHcX
76–78.25 and 79.75–81.25	500 m: NH Indian Ocean 2500 m: NH or SH Indian Ocean	NHIO	NHmT
81.25–82 and	500 m: Arabian Sea/coastal India	AS/CI	NHmT
85–88.75	2500 m: Arabian Sea/coastal India or Indian subcontinent		NHcT

[a]Also shown are the 500 and 2500 m trajectory information and characterization of the air mass regions.
[b]SHmX, southern hemisphere marine extratropical; SHmT, southern hemisphere marine tropical; NHmT, northern hemisphere marine tropical; NHcT, northern hemisphere continental tropical; NHcX, northern hemisphere continental extratropical.
[c]Trajectory arrival height to the ship location in meters.

for the measurement of aerosol chemical, physical, and optical properties; sunphotometers for the measurement of aerosol optical depth; and a lidar for the measurement of aerosol vertical profiles). This paper presents, as a function of aerosol source region, the measured chemical and optical properties and the relative significance of the dominant aerosol chemical components in radiative forcing.

[4] On the basis of air mass back trajectories and aerosol number concentrations and size distributions, eight air mass source regions impacted the samples collected on the *Ronald H. Brown*. The geographical regions along the cruise track where air masses from the different source regions were sampled are shown in Figure 1. Also shown are the prevailing trajectories for each geographical and air mass source region. Time periods when air masses from the different source regions were encountered along the cruise track are listed in Table 1. Several of the air mass source regions overlap in space but not in time as transport patterns changed each time the ship moved through the different geographical regions. The eight air mass source regions are the southern hemisphere Atlantic (SHAtl); southern hemisphere Indian Ocean (SHIO); northern hemisphere Indian Ocean (NHIO); east Indian subcontinent (EIndSub) where trajectories came from the northeast near Calcutta, through the southern portion of India, and then to the ship; Indian subcontinent (IndSub) where trajectories came from the northeast across central India to the ship; Arabia; Arabia/Indian subcontinent (Arabia/IndSub), a mixed region where lower-level trajectories came from Arabia and upper-level trajectories came from the northeast across India; and Arabian Sea/coastal India (AS/CI) where trajectories came from the north to northwest along the coast of India to the ship. The ship ventured into the Bay of Bengal near the end of the cruise, but instrumental problems and the limited number of samples collected made it difficult to characterize the region. Therefore it is omitted from the analysis presented here.

[5] Presented here are the concentrations and mass fractions of the chemical components (mass fraction is defined as the component concentration divided by the total aerosol mass concentration), the fraction of measured extinction due to each component, and mass extinction efficiencies of the chemical components for the different air mass regions. The chemical components considered include non-sea-salt (nss) sulfate aerosol, sea salt, particulate organic matter (POM), black carbon (BC), and inorganic oxidized material (IOM). Also presented for the source regions are average aerosol scattering and absorption coefficients, the backscattered fraction, Ångström exponent, and aerosol optical depth.

[6] An overdetermined data set allowed closure tests to be performed between measured and calculated parameters including aerosol mass (measured gravimetrically, derived from chemical analysis, and estimated from the number size distribution) and aerosol light extinction and single scattering albedo (derived from measured light scattering and absorption coefficients and calculated from Mie theory). Hence it was possible to test for consistency in the input data to the Mie calculations required for deriving the percent of extinction due to each chemical component and to assess the accuracy of the results of those calculations. In addition, mass extinction efficiencies were calculated with two independent methods (Mie calculations and a multiple linear regression). Results of these comparisons for each air mass source region are presented.

2. Measurements

2.1. Aerosol Sample Inlet

[7] Sample air for the chemical and optical measurements was drawn through a 6-m sample mast. The entrance to the

mast was 18 m above sea level and forward of the ship's stack. To maintain nominally isokinetic flow and minimize the loss of supermicron particles, the inlet was rotated into the relative wind. Air entered the inlet through a 5-cm diameter hole, passed through an expansion cone, and then into the 20-cm diameter sampling mast. The flow through the mast was 1 m^3 min^{-1}.

[8] The last 1.5 m of the mast were heated to establish a stable reference relative humidity (RH) for the sample air of 55 ± 5%. A stable reference RH allows for constant instrumental size segregation in spite of variations in ambient RH and results in chemical, physical, and optical measurements which are directly comparable. In addition, measurement at a constant reference RH makes it possible, with the knowledge of appropriate growth factors [*Clarke et al*., 2002], for end users of the data set (process, chemical transport, and radiative transfer models) to adjust the measured parameters to a desired relative humidity. A reference RH of 55% was chosen because it has been shown to reduce impactor bounce since there is enough water associated with the hygroscopic aerosol species at this RH to make the aerosol "sticky" (P. K. Quinn, unpublished results, 1995). In addition, for the atmospheric conditions encountered during INDOEX, it was possible to maintain 55% RH without excessive heating of the aerosol. On average, the aerosol was heated 5.4°C above the ambient temperature. All results except aerosol optical depth are reported at 55 ± 5% RH.

[9] Individual 1.9 cm diameter stainless steel tubes extended into the heated portion of the mast. These were connected to the aerosol instrumentation and impactors with graphite-polyethylene conductive tubing to prevent the electrostatic loss of particles. An exception to this was the lines connected to the impactors used for collection of carbonaceous aerosol; they were constructed of stainless steel. Air was sampled only when the concentration of particles greater than 15 nm in diameter indicated the sample air was free of local contamination (i.e., there were no rapid increases in particle concentration), the relative wind speed was greater than 3 m s^{-1}, and the relative wind was forward of the beam.

2.2. Regional Concentrations of Inorganic Ions

[10] Two-stage multijet cascade impactors [*Berner et al*., 1979] sampling air at 55 ± 5% RH were used to determine the submicron and supermicron concentrations of Cl^-, NO_3^-, $SO_4^=$, methanesulfonate (MSA^-), Na^+, NH_4^+, K^+, Mg^{+2}, and Ca^{+2}. Sampling periods ranged from 4 to 6 hours. The RH of the sampled airstream was measured a few inches upstream from the impactor. The 50% aerodynamic cutoff diameters $D_{50,aero}$ were 1.1 and 10 μm. Throughout the paper, submicron refers to particles with $D_{aero} < 1.1$ μm at 55% RH, and supermicron refers to particles with 1.1 $\mu m < D_{aero} < 10$ μm at 55% RH. Sub-10 μm refers to particles with $D_{aero} < 10$ μm at 55% RH.

[11] The 12 μm grease cup at the inlet of the impactor was coated with silicone grease to prevent the bounce of larger particles onto the downstream stages. A Tedlar film placed on the impactor jet plate having a $D_{50,aero}$ of 10 μm was sprayed with silicone lubricant for the same reason. Since films placed on downstream jet plates were used for chemical analysis, they were not sprayed to avoid unnecessary contamination. Tedlar films were used as the collection substrate in the impaction stage, and a Millipore Fluoropore filter (1.0-μm pore size) was used for the backup filter. Films were cleaned in an ultrasonic bath in 10% H_2O_2 for 30 min, rinsed in distilled, deionized water, and dried in an NH_3- and SO_2-free glove box. Filters and films were wetted with 1 mL of spectral grade methanol. An additional 5 mLs of distilled deionized water were added to the solution, and the substrates were extracted by sonicating for 30 min. The extracts were analyzed by ion chromatography [*Quinn et al*., 1998]. All handling of the substrates was done in the glove box. Blank levels were determined by loading an impactor with substrates but not drawing any air through it.

[12] Non-sea-salt sulfate concentrations were calculated from Na^+ concentrations and the ratio of sulfate to sodium in seawater. Sea-salt aerosol concentrations were calculated as

$$\text{sea salt } (\mu g\ m^{-3}) = Cl^-(\mu g\ m^{-3}) + Na^+(\mu g\ m^{-3}) \times 1.47, \quad (1)$$

where 1.47 is the seawater ratio of ($Na^+ + K^+ + Mg^{+2} + Ca^{+2} + SO_4^= + HCO_3^-$)/$Na^+$ [*Holland*, 1978]. This approach prevents the inclusion of non-sea-salt K^+, Mg^{+2}, Ca^{+2}, $SO_4^=$, and HCO_3^- in the sea-salt mass and allows for the loss of Cl^- mass through Cl^- depletion processes. It also assumes that all measured Na^+ and Cl^- are derived from seawater. Results of *Savoie and Prospero* [1980] indicate that soil dust has a minimal contribution to measured soluble sodium concentrations.

[13] Uncertainties of the ionic chemical components at the 95% confidence level were propagated as a quadratic sum of all errors involved which assumes that all errors were random. Details of the uncertainty analysis are given by *Quinn et al*. [2000a]. The form of the uncertainty equations in the work of *Quinn et al*. [2000a] were used for all uncertainty analyses in this paper.

2.3. Regional Concentrations of Total Organic and Black Carbon

[14] Three-stage multijet cascade impactors [*Berner et al*., 1979] sampling air at 55 ± 5% RH were used to determine submicron and supermicron concentrations of total, organic, and black carbon [*Neusüss et al*., 2002]. The impactor had $D_{50,aero}$ of 0.18, 1.1 and 10 μm. Only in this case does submicron refer to $0.18 < D_{aero} < 1.1$ μm. The 0.18 μm jet plate was used instead of a quartz backup filter to minimize positive artifacts due to the absorption of gas phase organics. With a jet plate, spot deposits of aerosol are collected which, when summed together, have less surface area than a quartz filter. In addition, the aluminum foils used as sampling substrates absorb less organic vapors than does a quartz filter [e.g., Turpin et al., 2000]. In addition, three samples were collected with a seven-stage impactor ($D_{50,aero}$ of 0.18, 0.31, 0.55, 1.1, 2.0, 4.1, and 10 μm) to obtain size distributions of OC and EC. Sampling periods ranged from 12 to 24 hours. Al foils were heated at the Institute for Tropospheric Chemistry (Leipzig, Germany) before the cruise at 600°C for 4 hours to remove organic contaminants. Blank levels were determined by placing substrates into a second impactor and deploying the impactor for the duration of the sampling period without drawing air through it. Foils were stored frozen until analysis.

[15] The samples were analyzed by a thermographic method using a commercial instrument (C-mat 5500, Ströhlein) at the Institute for Tropospheric Research (IfT) in Leipzig, Germany [*Neusüss et al*., 2000]. The sample was placed in a quartz tube and heated rapidly to a specific temperature. To separate organic carbon (OC) and BC, the sample was first heated to 590°C under nitrogen. The carbon compounds that

evaporate under these conditions are referred to as OC. Then the sample was heated under oxygen to 650°C, and all carbon except carbonate was oxidized. The evaporated carbon is completely oxidized to CO_2 followed by analysis with an IR detector. External standards were used to calibrate the measurements. As with all thermal carbon measurements, the OC/BC split is a method dependent property. The BC concentrations represent an upper limit as no correction for charring of organic matter was made.

[16] The mass of particulate organic matter (POM) was determined by multiplying the measured organic carbon concentration in μg C m^{-3} by a POM factor which is an estimated average of the molecular weight per carbon weight for the organic aerosol. A POM factor of 1.6 was used for all samples based on a review of published measurements of the composition of organic aerosol in urban and nonurban regions [*Turpin and Lim*, 2001]. The POM factor was assigned an absolute uncertainty of 0.35.

[17] The uncertainties associated with positive and negative sampling artifacts can be substantial [*Turpin et al*., 1994, 2000]. An effort was made to minimize positive artifacts by collecting samples on impaction plates. Negative artifacts may have occurred as a result of the pressure drop across the impactor (9 mbar for the 1.1 μm jet plate and 530 mbar for the 0.18 μm jet plate). No attempt was made to correct for artifacts or to determine their associated uncertainties since the information to do so was not available.

[18] The uncertainties for BC at the 95% confidence level were based on a quadrature sum of the uncertainty in the air volume sampled and 2 times the standard deviation of the blank values measured over the course of the experiment. The uncertainties for POM were based on a quadrature sum of the uncertainty in the air volume sampled, the uncertainty in the OC to POM conversion factor, and 2 times the standard deviation of the blank over the course of the experiment.

2.4. Regional Concentrations of IOM and Residual Mass

[19] Total elemental composition (Na, Mg, Al, Si, P, Cl, K, Ca, Ti, V, Cr, Mn, Fe, Ni, Cu, Zn, Ba, As, and Pb) was determined by thin-film X-ray primary and secondary emission spectrometry [*Feely et al*., 1991, 1998] at NOAA Pacific Marine Environmental Laboratory (PMEL). Submicron samples were collected on Nuclepore filters (0.4 μm pore size) mounted in a Berner impactor downstream of the $D_{50,aero}$ 1.1 μm jet plate. Bulk samples were collected on Nuclepore filters (0.4 μm pore size) in a filter pack having an upper $D_{50,aero}$ of 10 μm. Supermicron elemental concentrations were determined by difference between the submicron and bulk samples. This method of sample collection allows for the sharp size cut of the impactor while collecting a thin film of aerosol necessary for the X-ray analysis. Sampling periods ranged from 12 to 24 hours.

[20] Filters were acid-washed before sample collection by soaking in 4 N HNO_3 for 24 hours and then 2% HCL for 24 hours with multiple rinses with distilled deionized water between treatments. Filters were weighed before and after sample collection as described below. Blank levels were determined by loading an impactor or filter pack with a filter but not drawing any air through it.

[21] A component composed of inorganic oxidized material (IOM) was constructed from the elemental data. The IOM most likely was composed of soil dust and/or fly ash. Elemental concentrations alone are not sufficient to discriminate between the two. Regional crustal and fly ash enrichment factors for Al, Fe, and Ti relative to Si were calculated and found to be less than 2 for all source regions; values significantly greater than one are required to determine if the element has a noncrustal (i.e., fly ash) or nonfly ash (i.e., crustal) source. To construct the IOM component, the mass concentrations of Al, Si, Ca, Fe, and Ti, the major elements in soil and fly ash, were combined. It was assumed that each element was present in the aerosol in its most common oxide form (Al_2O_3, SiO_2, CaO, K_2O, FeO, Fe_2O_3, TiO_2) [*Seinfeld*, 1986]. The measured elemental mass concentration was multiplied by the appropriate molar correction factor as follows [*Malm et al*., 1994; *Perry et al*., 1997]:

$$[\mathrm{IOM}] = 2.2[\mathrm{Al}] + 2.49[\mathrm{Si}] + 1.63[\mathrm{Ca}] + 2.42[\mathrm{Fe}] + 1.94[\mathrm{Ti}]\,. \quad (2)$$

This equation includes a 16% correction factor to account for the presence of oxides of other elements such as K, Na, Mn, Mg, and V that are not included in the linear combination. In addition, the equation omits K from biomass burning by using Fe as a surrogate for soil K and an average K/Fe ratio of 0.6 in soil [*Cahill et al*., 1986]. The concentration of residual mass was calculated from the gravimetric mass minus the sum of the chemically analyzed species (ionic, POM, BC, and IOM).

[22] Uncertainties at the 95% confidence level associated with the IOM component were propagated as a quadratic sum of all errors involved including those due to the X-ray analysis, blank approximation, and volume of air sampled. XRF analysis errors are based on 2 times the standard deviation of 15 replicate analyses of a sample filter. Blank errors are based on 2 times the standard deviation of the average of all blanks collected over the course of the experiment. Uncertainties for the residual mass were propagated as a quadratic sum of the errors associated with the gravimetric, ionic, POM, BC, IOM, and calculated water mass.

2.5. Regional Mass Fractions

[23] Submicron and supermicron regional mass fractions were calculated from concentrations of the measured chemical components and the XRF Nuclepore filters that were weighed before and after sample collection. The filters were weighed at PMEL with a Cahn Model 29 microbalance housed in a glove box kept at a humidity of 33 $\pm$ 2%. The resulting mass concentrations from the gravimetric analysis include the water mass that is associated with the aerosol at 33% RH. Additional water mass may also be present due to interactions between the collected aerosol and the sampling substrate. The response of particles collected on a filter to changes in RH has been shown to be different than that of individual particles or bulk solutions of similar chemical composition [*McInnes et al*., 1996].

[24] The glove box was continually purged with room air that had passed through a scrubber of activated charcoal, potassium carbonate, and citric acid to remove gas phase organics, acids, and ammonia. Static charging, which can result in balance instabilities, was minimized by coating the walls of the glove box with a static dissipative polymer (Tech Spray, Inc.), placing an antistatic mat on the glove box floor, using antistatic gloves while handling the substrates, and exposing the substrates to a ^{210}Po source to dissipate any charge that had built up on the substrates. Before and after sample collection, substrates were stored double-bagged with the outer bag containing citric acid to prevent absorption of gas phase ammonia. More details of the weighing procedure are given by *Quinn and Coffman* [1998].

[25] Uncertainties of the mass fractions at the 95% confidence level were based on a quadratic sum of the uncertainties of the chemical concentrations and the gravimetrically determined mass. Uncertainty in the latter includes errors due to weighing, storage and transport, and the volume of air sampled [*Quinn et al*., 2000a]. To maintain the sampling RH of 55%, the sample air was heated, on average, 5.4°C (range of heating was 2° to 10°C). This heating may have led to the volatilization of a portion of the semivolatile organics and ammonium nitrate from the substrate thereby resulting in artificially low masses. Heating by 30°C has been found to result in a mass loss of about 34% for an aerosol dominated by wood smoke [*Meyer et al*., 1992; *Ayers et al*., 1999]. We expect the volatilization losses to be considerably less here since the aerosol was heated, on average, only 5.4°C (compared to 30°C); wood smoke, which contains significant quantities of semivolatile organics, was not the primary aerosol source; and ammonium nitrate contributed to less than 1% of the aerosol mass. It was not possible to quantify volatilization losses, however, since the composition of the semivolatile organics was unknown.

2.6. Aerosol Scattering, Backscattering, and Absorption Coefficients

[26] Measurements of aerosol scattering and hemispheric backscattering coefficients were made with an integrating nephelometer (Model 3563, TSI Inc.) at wavelengths of 450, 550, and 700 nm at 55 ± 5% RH. The RH was measured inside the nephelometer sensing volume. Two single-stage impactors, one with a $D_{50,\mathrm{aero}}$ of 1.1 μm and one with a $D_{50,\mathrm{aero}}$ of 10 μm, were placed upstream of the nephelometer. An automated valve switched between the two impactors every 15 min so that sampling alternated between sub-1 μm and sub-10 μm aerosol. Values measured directly by the nephelometer were corrected for an offset determined by measuring filtered air over a period of several hours [*Anderson and Ogren*, 1998]. In addition, they were corrected for the angular nonidealities, including truncation errors and nonlambertian response, of the nephelometer using

$$\sigma_{sp} = \sigma_{sp\_Meas} x \frac{\sigma_{sp\_True}}{\sigma_{sp\_Neph\_sim}}, \quad (3)$$

where σ_{sp_True} is the "true" scattering coefficient determined from the measured number size distribution and chemistry and a Mie scattering model and $\sigma_{sp\_Neph\_sim}$ is the nephelometer simulated scattering coefficient determined from a Mie scattering model which employs a Mie integral modified to simulate the nephelometer response [*Quinn and Coffman*, 1998]. (The Mie calculations are discussed in more detail below.) This correction is similar to that of *Anderson and Ogren* [1998] but uses the simultaneously measured size distribution rather than an assumed size distribution. Values are reported at 0°C and 1013 mbar.

[27] Sources of uncertainties associated with the use of the integrating nephelometer include photon counting during measurement, zeroing, and calibration; literature values of calibration gas scattering coefficients; variations in gas density within the nephelometer, and the angular correction applied in equation (3). These uncertainties were estimated using the method of *Anderson et al*. [1999]. Additional uncertainties include variations in measured scattering due to RH changes within the nephelometer sensing volume and inlet losses of large particles [*Quinn and Coffman*, 1998]. For a 30 min averaging time and a wavelength of 550 nm, a quadrature sum of errors yielded absolute uncertainties of 4.1 and 20 Mm^{-1} corresponding to low and high values of σ_{sp} equal to 24 and 110 Mm^{-1}, respectively. Absolute uncertainties for σ_{bsp} equal to 3.0 and 13 Mm^{-1} were 0.32 and 1.3 Mm^{-1}, respectively.

[28] The absorption coefficient for sub-1 μm aerosol, σ_{ap}, was measured at 55 ± 5% RH by monitoring the change in transmission through a filter with a Particle Soot Absorption Photometer (PSAP, Radiance Research). Measured values were corrected for a scattering artifact, the deposit spot size, the PSAP flow rate, and the manufacturer's calibration as per *Bond et al*. [1999]. Values are reported at 550 nm, 0°C, and 1013 mbar. Sources of uncertainty in the PSAP measurement include noise, drift, correction for the manufacturer's' calibration, and correction for the scattering artifact [*Anderson et al*., 1999]. A quadrature sum of these errors yields absolute uncertainties of 0.38 and 2.8 Mm^{-1} for σ_{ap} equal to 0.68 and 13 Mm^{-1}, respectively, for a 30 min averaging time.

2.7. Number Size Distribution

[29] Size distributions from 20 nm to 5 μm were measured with the combination of a differential mobility particle sizer (DMPS, University of Vienna (Reischle) medium column) and an aerodynamic particle sizer (APS) (TSI 3300) [*Bates et al*., 2002]. The DMPS was operated at 55 ± 5% RH. The APS was operated dry; diameters were shifted to 55% RH using the mass of water calculated to be associated with the aerosol at that RH (see section 3.1 for details of water calculation). Filtered mobility distributions from the DMPSs were converted to number size distributions using the inversion routine of *Stratman and Wiedensohler* [1997]. Data were corrected for diffusional losses [*Covert et al*., 1997] and size-dependent counting efficiencies [*Wiedensohler et al*., 1997].

[30] During INDOEX the integrated number concentration from the DMPS was 18 ± 10% lower than the total number measured by a TSI 3010 condensation particle counter (CPC). Two TSI 3010 counters run in parallel agreed to within 3.6 ± 9.5% (mean plus or minus one standard deviation of the ratio) yielding confidence in the CPC data. In addition, the number concentration derived from the DMPS is very sensitive to stability in instrument flow rates. A relative drift of 1% in the sheath to excess flow translates into a 10% change in the DMPS inlet flow and thus a 10% change in number concentration. A change in inlet flow also affects the DMPS transfer function and raises the error to 15% [*Bates et al*., 2002]. Because of the greater uncertainty in the DMPS number concentration relative to the CPC number concentration, the DMPS data were normalized using the 30 min average ratio of the total number concentration to the integrated DMPS number concentration.

[31] APS diameters were converted to geometric diameters by dividing by the square root of the particle density determined from the size-resolved chemical measurements. See section 3.1 for a description of the density calculations. An interactive routine was used to fit lognormal curves to the different modes of the number size distribution [*Quinn and Coffman*, 1998]. Surface area fit parameters for the total aerosol based on the number size distribution measured at 55 ± 5% RH are given in Table 2.

[32] Uncertainties in the measured number size distribution (and mass concentrations derived from the number size distribution) result from instrumental errors of particle sizing and counting due to flow instabilities in the DMPS and APS.

Table 2. Accumulation and Coarse Mode Surface Area Fit Parameters (Mean Values and 1σ Standard Deviation) at 55% RH

	Accumulation Mode			Coarse Mode I			Coarse Mode II		
Region	S, μm cm^{-3}	D_g, μm	σ_g	S, μm cm^{-3}	D_{gs}, μm	σ_g	S, μm cm^{-3}	D_g, μm	σ_g
SH Atlantic	11 ± 2.4	0.17 ± 0.01	1.3 ± 0.03	12 ± 11	0.79 ± 0.34	1.7 ± 0.63	34 ± 14	2.4 ± 0.24	1.7 ± 0.19
SH Indian Ocean	12 ± 4.1	0.25 ± 0.02	1.4 ± 0.12	16 ± 9.1	2.1 ± 0.21	1.9 ± 0.10			
NH Indian Ocean	44 ± 12	0.27 ± 0.03	1.6 ± 0.05	29 ± 3.9	2.2 ± 0.09	1.7 ± 0.06			
East Indian subcontinent	180 ± 8.1	0.36 ± 0.01	1.3 ± 0.02	11 ± 1.9	1.9 ± 0.05	1.7 ± 0.02			
Indian subcontinent	130 ± 35	0.32 ± 0.02	1.4 ± 0.05	11 ± 3.0	1.8 ± 0.09	1.6 ± 0.02			
Arabia	52 ± 7.6	0.26 ± 0.02	1.7 ± 0.11	24 ± 8.0	2.3 ± 0.09	1.7 ± 0.04			
Arabia - Indian subcontinent	120 ± 31	0.29 ± 0.02	1.5 ± 0.05	25 ± 5.2	2.0 ± 0.15	1.6 ± 0.04			
Arabian Sea-coastal India	79 ± 24	0.30 ± 0.01	1.4 ± 0.06	6.7 ± 3.6	1.7 ± 0.22	1.6 ± 0.04			

[a]The coarse aerosol was fit with two lognormal modes in SH Atlantic region to accommodate a bimodal structure. The two-mode fit results in the best representation of both the total surface area concentration and the mean diameter of the coarse aerosol [*Quinn and Coffman*, 1998].

The amount of observed drift in the sheath and excess flows led to a ± 20% uncertainty in the number concentration [*Bates et al*., 2002]. Additional factors affecting the accuracy of the conversion of the number concentration to a mass concentration include errors in the measured chemical composition and calculated density. Overall uncertainties in the submicron mass concentration derived from the number size distribution are ± 35% for a concentration of 3 μg m^{-3} [*Quinn and Coffman*, 1998]. Uncertainties for supermicron mass concentrations are ± 25% for a concentration of 20 μg m^{-3}.

2.8. Aerosol Optical Depth

[33] A five-channel (380, 440, 500, 675, and 870 nm) handheld Microtops sunphotometer (Solar Light Co.) was used to derive aerosol optical depth τ_a at 500 nm for the SHAtl region. It also was used to derive Ångström exponents å at 440 and 675 nm for all of the source regions. The instrument has built-in pressure and temperature sensors and was operated with a Global Positioning System (GPS) connection to obtain position and time of the measurements. A Matlab routine used by the NASA SIMBIOS program and Brookhaven National Laboratory was used to convert the raw signal voltages to aerosol optical depths. Included in the conversion is a correction for Rayleigh scattering [*Penndorf*, 1957], ozone optical depth, and an air mass that accounts for the Earth's curvature [*Kasten and Young*, 1989]. Ozone column amounts used to calculate the ozone optical depth were based on TOMS level 3 data for the locations and time periods of the cruise. The instrument was calibrated using a Langley plot approach [*Shaw*, 1983] by the manufacturer prior to the cruise and again at Mauna Loa 5 months after the cruise. Calibration constants for the five wavelengths differed by less than 0.9% between the two calibrations, which corresponds approximately to 0.01 in optical depth.

[34] In addition, aerosol optical depth at 500 nm and Ångström exponents at 415 and 862 nm were derived from a fast-rotating shadowband radiometer (FFSR, Yankee Environmental Systems, Inc.). The FFSR, being an automated instrument, was able to provide more data points throughout the cruise. Unfortunately, FFSR measurements were not available during the SHAtl region. A Brookhaven National Laboratory marine version was used. In the marine version the electrical response time is decreased to about 1 ms [*Reynolds et al*., 2001] to accommodate for the motion of the ship. The instrument calibration coefficients for the cruise were determined using the Langley plot technique at Mauna Loa. Additional calibrations were performed during the cruise that showed good agreement with the Mauna Loa data. The accuracy of the calibration coefficients is ±5%, and the accuracy of the irradiance measurements is ±6%. A regression of aerosol optical depth at 500 nm from the Microtops sunphotometer versus the FFSR resulted in a coefficient of determination, r^2, of 0.92 and a slope of 1.02.

2.9. Ancillary Parameters

[35] Also measured were meteorological parameters including surface temperature, RH, wind speed and direction, as well as vertical profiles of these parameters from radiosondes. Air mass back trajectories were calculated for three arrival altitudes (500, 2500, and 5500 m) for the ship's position at 6 hour intervals. Trajectories were calculated with the hybrid single-particle Lagrangian integrated model HY-SPLIT 4 based on the FNL global wind field [*Draxler*, 1992; http://www.noaa.gov/ready-bin/fnl.pl]

3. Model Calculations

3.1. Calculation of Aerosol Water Mass, Density, and Refractive Index

[36] The gravimetric analysis was performed at 33 ± 3% RH. Hence the measured mass on the filter substrates included the amount of water associated with the aerosol at that RH. The impactors, nephelometer, and PSAP sampled aerosol at 55 ± 5% RH. The chemical thermodynamic equilibrium model AeRho [*Quinn et al*., 1998; *Quinn and Coffman*, 1998] was used to estimate the water mass associated with the inorganic ions at 33 and 55% RH so that the gravimetric and chemically analyzed mass could be adjusted to the RH of the optical measurements.

[37] No information was available on the chemical composition or hygroscopicity of the organic mass. Without this information it is difficult to estimate the water mass associated with the organic matter or to estimate the error imposed by this assumption on calculated extinction. There is no consensus on the direction or magnitude of the contribution by organics to total aerosol water. Empirical evidence exists indicating that

organics enhance water absorption by aerosols at high RH under nonurban conditions and diminish water absorption under urban conditions [*Saxena et al*., 1995]. *Dick et al*., [2000] showed that organic-associated water content is considerably less than that of sulfate compounds, on a volume basis, for high RH but comparable or greater for low RH. Model estimates indicate that the contribution of secondary organic aerosols (SOA) to total aerosol water is less than 5% for cases when SOA make up 22% of the total particle mass less than 2.5 μm in diameter [*Ansari and Pandis*, 2000]. The suppression of light scattering at high RH ($>$ 70%) has been attributed to the presence of organic aerosols [*McInnes et al*., 1998]. Given this state of knowledge and the lack of information on the chemical composition of the organic matter, no attempt was made to calculate its associated water mass or to estimate the error due to the assumption that organic-associated water mass was negligible. The trace element components estimated from the XRF analysis also were assumed to be hygrophobic.

[38] Using the aerosol chemical composition measured with seven-stage multijet cascade impactors [*Berner et al*., 1979] ($D_{50,aero}$ of 0.18, 0.31, 0.55, 1.1, 2.0, 4.1, and 10 μm), AeRho also was used to calculate the refractive index at 550 nm and density of the mix of all aerosol components (for the calculation of total extinction) and for the individual chemical components (for the calculation of extinction fractions and mass extinction efficiencies). Details of the AeRho calculations are given below.

[39] For the purpose of reconciling all the various in situ measurements, AeRho is a static model. It is designed to take the measured ionic composition of the aerosol and the constant sampling RH and to determine the molecular composition of the ionic chemical species within the aerosol. The molecular composition then is used to calculate the water mass associated with the aerosol and the aerosol refractive index and density. The model is not used to describe a dynamic system in which changes in the concentration of gas phase species affect the aerosol molecular composition. Therefore the model does not include interactions between the gas and aqueous phases. In addition, because of the constant sampling RH, it is not necessary to take into account changes in particle size with changes in RH.

[40] For the calculation of total extinction the aerosol was assumed to be an internal mixture containing all measured chemical components. The chemical reactions allowed to occur are shown in Table 3. The ionic molalities for each of the input species are determined initially by assuming that the activity of water is equal to the instrumental RH. Then, using the ZSR method [*Zdanovskii*, 1936; *Robinson and Stokes*, 1965], a further approximation of the water content of the aerosol is made. Aqueous phase concentrations are activity corrected using the method of *Bromley* [1973] which allows for the prediction of activity coefficients of strong electrolytes in multielectrolyte solutions based on binary solution activity coefficients [*Pilinis and Seinfeld*, 1987]. The pure-solution binary activity coefficients are calculated using the method of *Pitzer and Mayorga* [1973]. The ionic species are partitioned between the solid and aqueous phases with the solids precipitating in the most thermodynamically favorable order. The crystallization RH used for each solid phase species is listed in Table 3. The remaining aqueous ionic species are converted to aqueous compounds in accordance with the thermodynamic equilibrium constants. Finally, thermodynamic equilibrium with respect to water is tested for, and the water activity is iterated until equilibrium is established.

Table 3. Chemical Reactions Included in the Chemical Equilibrium Model AeRho

Reaction	Crystallization RH
$2H^+_{(aq)} + SO_4^=_{(aq)} \leftrightarrow H_2SO_{4(aq)}$	
$H^+_{(aq)} + HSO_4^=_{(aq)} \leftrightarrow H_2SO_{4(aq)}$	
$2NH_4^+_{(aq)} + SO_4^=_{(aq)} \leftrightarrow (NH_4)_2SO_{4(aq)}$	
$NH_4^+_{(aq)} + HSO_4^=_{(aq)} \leftrightarrow NH_4HSO_{4(aq)}$	
$2Na^+_{(aq)} + SO_4^=_{(aq)} \leftrightarrow Na_2SO_{4(aq)}$	
$Na^+_{(aq)} + HSO_4^=_{(aq)} \leftrightarrow NaHSO_{4(aq)}$	
$2K^+_{(aq)} + SO_4^=_{(aq)} \leftrightarrow K_2SO_{4(aq)}$	
$K^+_{(aq)} + HSO_4^=_{(aq)} \leftrightarrow KHSO_{4(aq)}$	
$H^+_{(aq)} + NO_3^-_{(aq)} \leftrightarrow HNO_{3(aq)}$	
$NH_4^+_{(aq)} + NO_3^-_{(aq)} \leftrightarrow NH_4NO_{3(aq)}$	
$Na^+_{(aq)} + NO_3^-_{(aq)} \leftrightarrow NaNO_{3(aq)}$	
$K^+_{(aq)} + NO_3^-_{(aq)} \leftrightarrow KNO_{3(aq)}$	
$H^+_{(aq)} + Cl^-_{(aq)} \leftrightarrow HCl_{(aq)}$	
$NH_4^+_{(aq)} + Cl^-_{(aq)} \leftrightarrow NH_4Cl_{(aq)}$	
$Na^+_{(aq)} + Cl^-_{(aq)} \leftrightarrow NaCl_{(aq)}$	
$K^+_{(aq)} + Cl^+_{(aq)} \leftrightarrow KCl_{(aq)}$	
$2NH_4^+_{(aq)} + SO_4^=_{(aq)} \leftrightarrow (NH_4)_2SO_{4(s)}$	40[a]
$NH_4^+_{(aq)} + HSO_4^=_{(aq)} \leftrightarrow NH_4HSO_{4(s)}$	22[a]
$2Na^+_{(aq)} + SO_4^=_{(aq)} \leftrightarrow Na_2SO_{4(s)}$	59[a]
$Na^+_{(aq)} + HSO_4^=_{(aq)} \leftrightarrow NaHSO_{4(s)}$	0.05[b]
$2K^+_{(aq)} + SO_4^=_{(aq)} \leftrightarrow K_2SO_{4(s)}$	62[c]
$K^+_{(aq)} + HSO_4^=_{(aq)} \leftrightarrow KHSO_{4(s)}$	62[c]
$NH_4^+_{(aq)} + NO_3^-_{(aq)} \leftrightarrow NH_4NO_{3(s)}$	32[b]
$Na^+_{(aq)} + NO_3^-_{(aq)} \leftrightarrow NaNO_{3(s)}$	30[b]
$K^+_{(aq)} + NO_3^-_{(aq)} \leftrightarrow KNO_{3(s)}$	62[c]
$NH_4^+_{(aq)} + Cl^-_{(aq)} \leftrightarrow NH_4Cl_{(s)}$	47[d]
$Na^+_{(aq)} + Cl^-_{(aq)} \leftrightarrow NaCl_{(s)}$	45[e]
$K^+_{(aq)} + Cl^-_{(aq)} \leftrightarrow KCl_{(s)}$	62[e]

[a] *Tang and Munkelwitz* [1994].
[b] *Tang* [1996].
[c] No data, assumed from KC1.
[d] *Cohen et al*. [1987].
[e] *Tang et al*. [1997].

[41] Polynomial fits based on data of *Tang and Munkelwitz* [1991, 1994] for metastable particles are used to estimate densities of individual inorganic soluble species. Data from *Bray* [1970] are used to estimate the density of H_2SO_4. The density of OC was assumed to be 1.4 g cm^{-3} [*Turpin and Lim*, 2001] and that of BC 2 g cm^{-3} [*Seinfeld and Pandis*, 1998]. For the purposes of the extinction calculations, the IOM and residual mass were combined into one component. The density of the component was set equal to that of a mixture of 45% montmorillonite (2.5 g cm^{-3}) and 55% kaolinite (2.6 g cm^{-3}) as these two minerals are common components of soil dust [*Sokolik and Toon*, 1999]. A volume-weighted average was taken of the density of the individual species to estimate the density of the aerosol mix in each impactor size bin. Average submicron and supermicron densities for each source region for the mix of aerosol chemical components are reported in Table 4.

[42] The method of partial molar refractions [*Stelson*, 1990] was used to calculate the real portion of the refractive index as a function of size at 550 nm. Values of the partial molar refractions of all chemical species except IOM were taken from [*Stelson*, 1990]. The complex refractive index at 550 nm was obtained by volume averaging the refractive index of the scattering and absorbing components. A refractive index of 1.5 was used for the IOM component based on the kaolinite-montmorillonite mixture at 550 nm [*Sokolik and Toon*, 1999]. Average submicron and supermicron refractive indices for

Table 4. Regional Averages of Submicron ($D_{aero} < 1.1$ μm) and Supermicron ($1.1 < D_{aero} < 10$ μm) Densities and Real and Imaginary Portions of the Refractive Index of the Bulk Aerosol Estimated From the Chemical Thermodynamic Equilibrium Model, AeRho[a]

	Density, cm^{-3}		Refractive Index			
			Real Portion		Imaginary Portion	
Region	Sub-μm	Super-μm	Sub-μm	Super-μm	Sub-μm	Super-μm
SH Atlantic	1.44	1.31	1.49	1.45	0	0
SH Indian Ocean	1.48	1.30	1.50	1.44	2.5E-3[b]	0
NH Indian Ocean	1.61	1.35	1.54	1.44	1.67E-2	0
East Indian subcontinent	1.57	1.50	1.54	1.44	5.21E-2	0
Indian subcontinent	1.70	1.69	1.54	1.46	4.95E-2	0
Arabia	1.64	1.63	1.52	1.46	1.09E-2	0
Indian subcontinent-Arabia	1.69	1.59	1.53	1.45	2.0E-2	0
Arabian Sea-coastal India	1.72	1.69	1.53	1.45	2.6E-2	0

[a]Values are reported for 55% RH and 550 nm.
[b]Read 2.5E-3 as 2.5×10^{-3}.

each source region for the mix of aerosol chemical components are reported in Table 4.

[43] For the calculation of the extinction due to each chemical component and mass extinction efficiencies, the method described above was followed but only individual components were considered. For components containing more than one chemical species (e.g., $H_2SO_4/NH_4HSO_4/(NH_4)_2SO_4$ in the nss sulfate aerosol), a volume-weighted average was taken of the density of the individual species to estimate the density of the component in each impactor size bin. Similarly, the method of partial molar refractions was used to calculate the real portion of the refractive index as a function of size for the water soluble chemical components containing more than one chemical species.

3.2. Calculation of Extinction Due to Each Chemical Component and Mass Extinction Efficiencies

[44] The chemical components considered in this analysis are sea salt, nss sulfate, IOM, POM, and BC. The sea-salt component includes all measured NO_3^- in the supermicron size range on the assumption that gas phase HNO_3 resulting from combustion processes reacts with sea salt to form $NaNO_3$ [*Clegg and Brimblecombe*, 1985]. Nss sulfate aerosol includes nss $SO_4^=$ and all measured NH_4^+ up to an NH_4^+ to nss $SO_4^=$ molar ratio of 2. The sea-salt and nss sulfate components also include the water calculated to be associated with these components at 55% RH. A combustion component composed of BC and submicron soluble nss K^+, nss $SO_4^=$ and NO_3^- was constructed whose refractive index and density were determined by mass averaging those of the individual species. The submicron nss $SO_4^=$ added to the combustion component was found by the equilibrium calculation to be in excess of an NH_4^+ to nss $SO_4^=$ molar ratio of 2. NO_3^- and nss $SO_4^=$, assumed here to be in the form of KNO_3 and K_2SO_4, have been measured in biomass burning plumes by *Liu et al.* [2000].

[45] Size distributions of sea salt, nss sulfate aerosol, POM, and the combustion component were determined from the seven-stage impactor measurements coupled with the number size distributions (see below). Since only submicron and supermicron samples were collected for the IOM component, it was distributed as sea salt. As discussed below in section 4.5, mass extinction efficiencies derived with the Mie calculational method fall within the range of those derived from an independent empirical multiple linear regression method. In addition, the values are within the range of those previously reported, indicating that the assumed IOM size distribution was reasonable.

[46] Using the output from AeRho, a volume ratio (component volume/total aerosol volume) was calculated for each component within each impactor size bin from the component mass concentration and density (both determined from AeRho) in the size bin. Component surface area ratios were then derived from the volume ratios. Extinction coefficients (σ_{ep}, Mm^{-1}) at 550 nm were calculated for each component using the total aerosol surface area fit parameters (from the measured number size distributions) and the component surface area ratios. Surface area fit parameters (as opposed to number or volume fit parameters) were found to give the most accurate representation of the aerosol when attempting to fit both the accumulation and coarse modes. Surface area fit parameters for the total aerosol based on the number size distribution measured at 55 ± 5% RH are given in Table 2. This approach uses the measured chemical information but maintains the higher size resolution of the measured number size distribution. Having acquired size distributions of σ_{ep} for each component, values of submicron and supermicron component σ_{ep} were determined by integrating over the appropriate size range. Mass extinction efficiencies ($m^2\ g^{-1}$) at 550 nm were calculated from the component $\sigma_{ep,j}$ (Mm^{-1}) and mass concentrations ($\mu g\ m^{-3}$) for the submicron, supermicron, and sub-10 μm size ranges.

4. Results

4.1. Closure Tests: Comparison of Measured and Calculated Aerosol Mass and Extinction

[47] Mean regional values of three measures of mass were compared to assess internal consistency in the impactor and number size distribution data used in the extinction calculations. Submicron and supermicron aerosol mass concentrations were determined gravimetrically, by summing the mass of the chemically analyzed species, and from the number size distribution using the density of the total aerosol mixture estimated with AeRho. The amount of water calculated to be associated with the aerosol at 55% RH was added to the

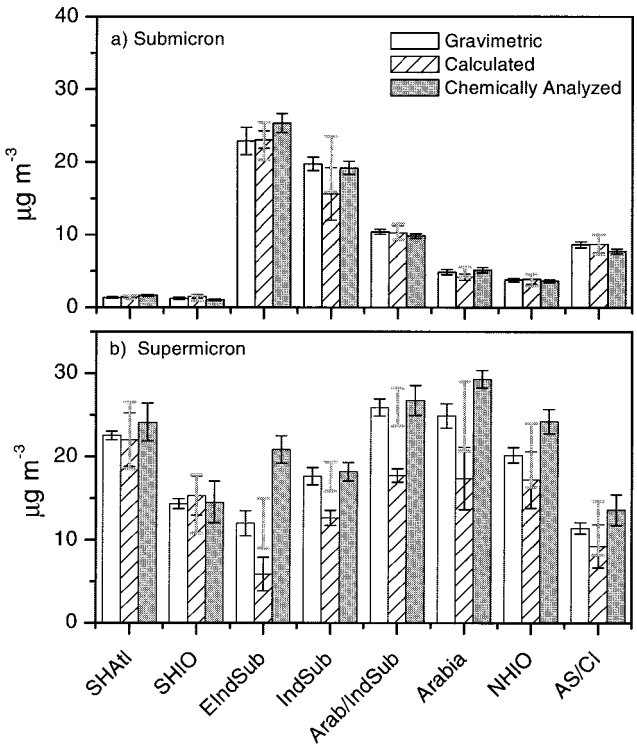

Figure 2. Comparison of three measures of the aerosol mass concentration at 55% RH for the (a) submicron and (b) supermicron size ranges. Gravimetric denotes the gravimetrically analyzed mass, and chemically analyzed is the sum of the mass analyzed for inorganic ions, organic (as POM) and black carbon, and trace elements (as IOM). Both the gravimetric and chemically analyzed mass include the water calculated to be associated with the inorganic ions at 55% RH. Calculated denotes the mass estimated from the number size distribution and the density based on the measured chemical composition. Black error bars indicate the 1σ standard deviation of the mean. Gray error bars indicate the overall experimental uncertainty for the mass closure experiment.

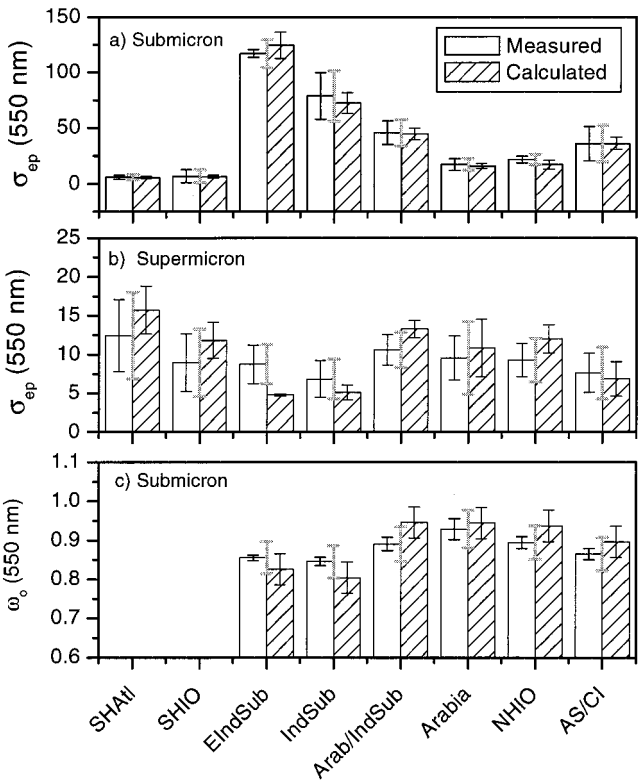

Figure 3. Comparison of the regional mean measured extinction (sum of the STP-corrected σ_{sp} from the nephelometer and σ_{ap} from the PSAP) and the calculated extinction (sum of the nephelometer-simulated σ_{sp} and the calculated σ_{ap}) for the (a) submicron and (b) supermicron size ranges. (c) Comparison of the measured and calculated submicron single scattering albedo for those air mass regions with measured σ_{ap} above the detection limit of 0.34 Mm^{-1} throughout the entire sampling period. All results are shown at 55% RH and 550 nm. Error bars are as in Figure 2.

gravimetric and chemically analyzed mass to adjust them to the measurement RH of the number size distribution.

[48] As shown in Figure 2, submicron mass concentrations from the three methods agreed for all source regions within the overall experimental uncertainty. Overall uncertainty was calculated from a quadrature sum of the uncertainties of the three methods [*Quinn and Coffman*, 1998]. This level of agreement gives confidence (for the submicron size range) to the density that was used to convert number to mass and the calculated water mass. In addition, it indicates that the chemical analyses accounted for all of the species that were present in the aerosol.

[49] Supermicron mass concentrations from the three methods agreed for source regions where the sampled air had been over the ocean and not over land for at least 6 days prior to reaching the ship (SHAtl, SHIO, NHIO, and AS/CI). For source regions where the sampled air had been over land in the 6 days prior to reaching the ship (EIndSub, IndSub, Arabia/IndSub, and Arabia), mass derived from the number size distribution was low relative to that determined gravimetrically and through chemical analyses. One factor responsible for the disagreement could be the calculated water values used to adjust the gravimetric and chemically analyzed mass to 55% RH. For the supermicron size range the calculated water is due primarily to sea salt aerosol. If the interaction of sea salt with other chemical components decreases the water uptake and/or retention by sea salt, calculated water values will be too high. These four source regions had relatively high concentrations of non-sea-salt supermicron mass.

[50] Extinction for submicron and supermicron aerosol was derived from the measured scattering and absorption coefficients. In addition, extinction was estimated using the measured chemical composition and number size distribution as input to Mie calculations. Measured and calculated submicron extinction agreed within the overall experimental uncertainty for all source regions (Figure 3). (The most direct comparison of the nephelometer-measured and nephelometer-simulated scattering coefficients was desired. Hence the comparison used the scattering coefficients measured directly by the nephelometer without an angular correction and the nephelometer-simulated scattering coefficients.) Agreement was obtained for the supermicron size range in all source regions except EIndSub despite the lack of supermicron mass closure in the EIndSub, IndSub, Arabia/IndSub, and Arabia regions. The amount of calculated water significantly affected the gravimetric and chemically analyzed mass (the added water made up 24 to 36% of the supermicron mass for the EIndSub, IndSub, Arabia/

Table 5. Concentrations, Standard Deviations ($\pm 1\sigma$), and Absolute Uncertainties (95% Confidence Level, Shown in Parentheses) of the Mean of Aerosol Ionic and Carbonaceous Submicron ($D_{aero} < 1.1$ μm at 55% RH) Chemical Species for the Different Air Mass Regions

	Concentration, $\mu g\ m^{-3}$					
Air Mass Region	nss $SO_4^=$	NH_4^+	Sea Salt	NO_3^-	POM[a]	BC[b]
SH Atlantic	0.31 ± 0.16 (0.01)	0.04 ± 0.03 (0.003)	0.17 ± 0.10 (0.05)	0.003 ± 0.008 (0.001)	0.16 ± 0.02 (0.04)	<0.01
SH Indian Ocean	0.52 ± 0.18 (0.01)	0.09 ± 0.04 (0.003)	0.07 ± 0.08 (0.02)	<0.001	0.07 ± 0.08 (0.04)	<0.01
NH Indian Ocean	1.8 ± 0.24 (0.03)	0.5 ± 0.12 (0.009)	0.09 ± 0.03 (0.03)	0.007 ± 0.007 (0.003)	0.13 ± 0.08 (0.06)	0.14 ± 0.05 (0.02)
East Indian subcontinent	13 ± 1.9 (0.32)	1.5 ± 0.06 (0.04)	0.10 ± 0.01 (0.05)	0.03 ± 0.02 (0.006)	1.4 ± 0.08 (0.19)	1.8 ± 0.23 (0.06)
Indian subcontinent	7.5 ± 2.2 (0.19)	2.1 ± 0.71 (0.05)	0.08 ± 0.02 (0.04)	0.02 ± 0.01 (0.006)	1.2 ± 0.13 (0.30)	1.4 ± 0.06 (0.08)
Arabia	1.5 ± 0.21 (0.04)	0.37 ± 0.04 (0.009)	0.13 ± 0.07 (0.04)	0.02 ± 0.01 (0.005)	0.78 (0.20)	0.08 (0.05)
Arabia-Indian subcontinent	3.9 ± 0.93 (0.05)	0.96 ± 0.25 (0.01)	0.09 ± 0.05 (0.02)	0.02 ± 0.008 (0.003)	0.94 ± 0.88 (0.10)	0.54 ± 0.36 (0.02)
Arabian Sea-coastal India	3.7 ± 1.3 (0.06)	0.90 ± 0.34 (0.21)	0.05 ± 0.03 (0.03)	0.02 ± 0.007 (0.004)	0.42 ± 0.20 (0.09)	0.38 ± 0.12 (0.02)

[a]Here $\mu g\ C\ m^{-3}$ of OC × 1.6.
[b]Here $\mu g\ C\ m^{-3}$.

IndSub, and Arabia regions). Water does not affect as directly the calculated aerosol refractive index and density that are required for the extinction calculations.

[51] As an additional check on the extinction calculations, measured and calculated single scattering albedos were compared for the submicron size range. The comparison was not done for the supermicron size range as absorption values were below the detection limit of 0.34 Mm^{-1}. As shown in Figure 3, agreement was within the overall experimental uncertainty for all source regions with detectable absorption.

[52] Agreement in extinction for submicron and supermicron size range indicates that the calculated extinction is accurate and lends confidence to the calculated extinction due to individual chemical components. Supermicron extinction fractions for those source regions where mass or extinction closure was not obtained, should be considered less certain, however.

4.2. Regional Chemical Composition and Mass Fractions

4.2.1. Sulfate Aerosol

[53] Table 5 lists the mean concentrations, standard deviations, and absolute uncertainties of the major submicron ionic chemical species for the different air mass source regions. Mean submicron nss $SO_4^=$ concentrations were lowest in the marine regions south of the ITCZ. SHAtl and SHIO nss $SO_4^=$ concentrations averaged 0.31 ± 0.16 and 0.52 ± 0.18 $\mu g\ m^{-3}$ (average and 1σ standard deviation), respectively. These concentrations are similar to the mean values observed for different latitude bands of the central Pacific (0.13 to 0.50 $\mu g\ m^3$ [*Quinn et al*., 2000a]) and the southern Atlantic (0.52 ± 0.14 $\mu g\ m^{-3}$ [*Quinn et al*., 2001; *Andreae et al*., 1995]). The NHIO region includes time periods when the ship was north of the ITCZ, within the ITCZ, and south of the ITCZ but with trajectories coming from the northern hemisphere. (The ITCZ was located between 2°S and 1°N when the ship first crossed it between 67° and 70°E on days 58 and 59. It was located between 5°S and 8°S when the ship crossed it at 73°E on days 76 to 79.) Mean nss $SO_4^=$ concentrations for this region were about a factor of 6 higher (1.8 ± 0.24 $\mu g\ m^{-3}$) than for regions south of the ITCZ and ranged from 1.5 to 2.2 $\mu g\ m^{-3}$. The highest concentrations of seawater dimethylsulfide (6.3 n*M*) and atmospheric dimethysulfide (370 pptv) (from which biogenic nss $SO_4^=$ is derived) were measured in the ITCZ suggesting that the elevated nss $SO_4^=$ for the NHIO region was, in part, biogenic in origin.

[54] On the basis of trajectories arriving at the ship location at a height of 500 m, lower-level air from three of the nonmarine source regions did not pass over the Indian subcontinent prior to reaching the ship. The mean nss $SO_4^=$ concentration for the Arabia region was comparable to the NHIO region (1.5 ± 0.21 $\mu g\ m^{-3}$). Mean values were higher for the Arabia/IndSub (3.9 ± 0.93 $\mu g\ m^{-3}$) and the AS/CI (3.7 ± 1.3 $\mu g\ m^{-3}$) regions. The Arabia/IndSub region experienced low-level (500 m) flow from Arabia and upper-level (2500 m) flow from the Indian subcontinent. Micropulse lidar measurements show the presence of lower and upper aerosol layers for this region with mixing between the two at times [*Welton et al*., 2002]. A portion of the nss sulfate aerosol measured at the surface may have resulted from mixing of the upper layer Indian subcontinent air mass into the boundary layer.

[55] Mean nss $SO_4^=$ concentrations were highest for the two source regions with lower-level flow from the Indian subcontinent. The IndSub region, during which air flowed from central India to the ship, had a mean nss $SO_4^=$ concentration of 7.5 ± 2.2 $\mu g\ m^{-3}$ with a range of 4.8 to 9.7 $\mu g\ m^{-3}$. The EIndSub region with air flow from the Calcutta region across southern Indian or Sri Lanka to the ship had a mean concentration of 13 ± 1.9 $\mu g\ m^{-3}$ and a range of 11 to 16 $\mu g\ m^{-3}$. The mean concentration measured in pollution plumes at altitudes less than 500 m off the east coast of the United States during TARFOX was 11 $\mu g\ m^{-3}$ with a range of 1 to 19 $\mu g\ m^{-3}$ [*Hegg et al*., 1997]. Regional mean NH_4^+ to nss $SO_4^=$ molar ratios ranged from 0.63 to 1.5 indicating that, on average, the sulfate aerosol was not completely neutralized by ammonium.

[56] Mass fractions and associated uncertainties at the 95% confidence level of the major submicron chemical species are shown in Figure 4. Mass fractions were calculated from the measured component mass concentration and the total aerosol mass concentration determined by gravimetric analysis. Nss sulfate aerosol, which includes nss $SO_4^=$, NH_4^+, and H_2O at 55% RH, made up the majority of the submicron mass in all source regions except the two most remote marine regions (SHAtl and SHIO). Even in these two regions, however, the sulfate mass fraction was substantial averaging 36 ± 12% for

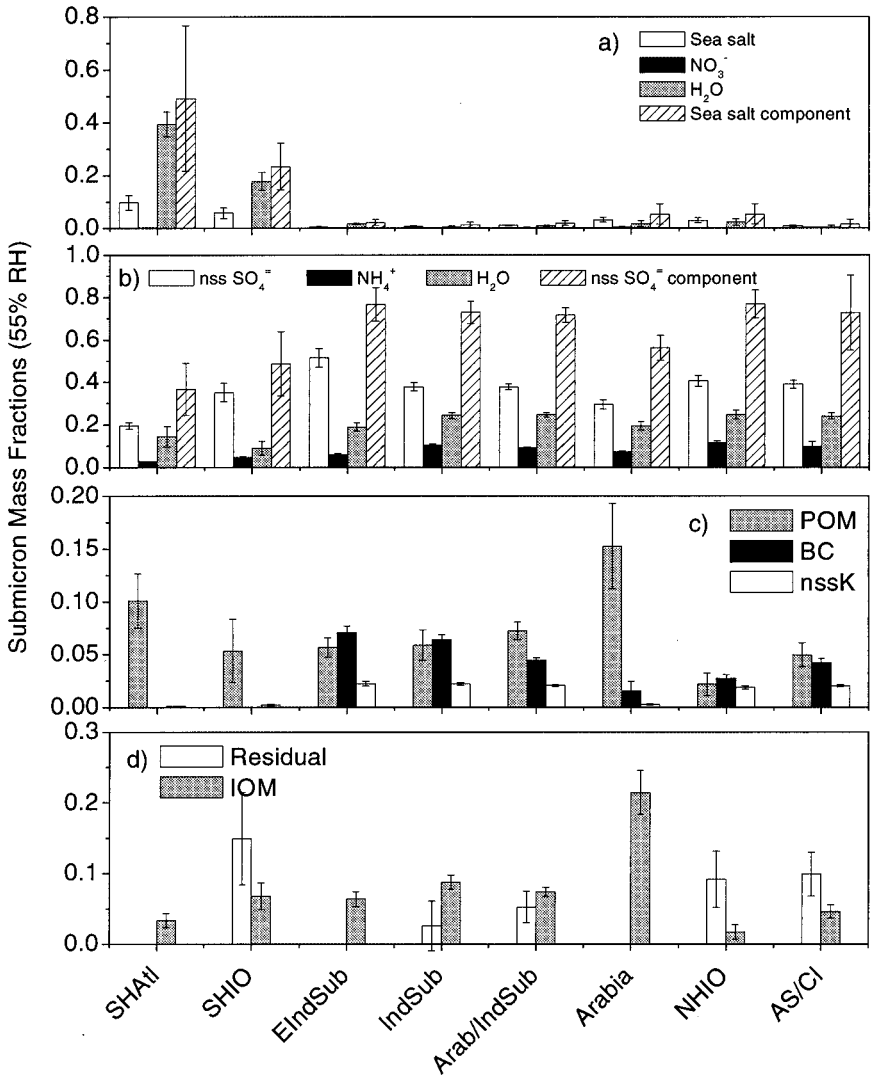

Figure 4. Regional mean submicron mass fractions of the dominant chemical components at 55% RH. Error bars indicate the uncertainty at the 95% confidence level. The sea-salt component mass includes sea salt and water. The nss sulfate component includes nss $SO_4^=$, NH_4^+, and water. The number of samples available for the mass fraction calculation in each region was as follows: SHAtl 6, SHIO 5, EIndSub 1, IndSub 2, Arabia/IndSub 5, Arabia 2, NHIO 3, AS/CI 3.

the SHAtl and 49 ± 15% (mean and uncertainty at the 95% confidence level) for the SHIO.

[57] Supermicron nss $SO_4^=$ concentrations were highest in the EIndSub (0.27 ± 0.42 $\mu g\ m^{-3}$) and IndSub (0.19 ± 0.14 $\mu g\ m^{-3}$) regions (see Table 6). In all other source regions, concentrations were less than 0.06 $\mu g\ m^{-3}$. Supermicron mean NH_4^+ concentrations were less than 0.03 $\mu g\ m^{-3}$ for all source regions. Supermicron mass fractions of nss sulfate aerosol ranged from undetectable to 2.2% (Figure 5).

4.2.2. Sea Salt and Nitrate

[58] Mean submicron sea-salt concentrations ranged between 0.05 and 0.17 $\mu g\ m^{-3}$ for all source regions (Table 5). These concentrations are low relative to those reported for latitude bins of the central Pacific (0.11 to 0.58 $\mu g\ m^{-3}$ [*Quinn et al.*, 2000a]), for different air mass types in the northeast Atlantic (0.34 to 0.88 $\mu g\ m^{-3}$ [*Quinn et al.*, 2000b), and for the remote Southern Ocean (1.0 ± 0.55 $\mu g\ m^{-3}$ [*Quinn et al.*, 1998]). They are comparable to concentrations reported for several different latitude bands of the Atlantic (0.08 to 0.22 $\mu g\ m^{-3}$ [*Quinn et al.*, 2001]. The low concentrations may have been due to the relatively low wind speeds during INDOEX that averaged 5.6 ± 2.8 m s^{-1}. For comparison, wind speeds for the Southern Ocean during ACE 1 averaged 9.5 m s^{-1} and for the northeast Atlantic during ACE 2 averaged 8.2 m s^{-1} [*Quinn et al.*, 2000b].

[59] Mass fractions of submicron sea-salt aerosol (including sea salt and the water associated with it at 55% RH) were high for the two remote marine source regions (49 ± 27% for the SHAt1 and 23 ± 8.8% for the SHIO). They were less than 2.5% for all other source regions. The low mass fractions are in contrast to what has been observed for remote regions of the central Pacific (7 to 53% [*Quinn et al.*, 2000a]) and marine and continentally impacted regions of the Atlantic (9 to 49% [*Quinn et al.*, 2001]).

[60] On a regional basis, mean supermicron sea-salt concentrations were either lower than or typical of those reported

Table 6. Concentrations, Standard Deviations ($\pm 1\sigma$), and Absolute Uncertainties (95% Confidence Level, Shown in Parentheses) of the Mean of Aerosol Ionic and Carbonaceous Supermicron (1.1 μm $< D_{aero} <$ 10 μm at 55% RH) Chemical Species for the Different Air Mass Regions

	Concentration, μg m^{-3}				
Air Mass Region	nss $SO_4^=$	NH_4^+	Sea Salt	NO_3^-	POM[a]
SH Atlantic	0.02 ± 0.03 (0.0004)	<0.001	10 ± 3.7 (0.13)	0.12 ± 0.15 (0.004)	0.22 ± 0.20 (0.04)
SH Indian Ocean	0.03 ± 0.07 (0.001)	<0.001	5.2 ± 3.7 (0.08)	0.17 ± 0.05 (0.004)	0.14 (0.05)
NH Indian Ocean	<0.001	<0.001	6.5 ± 1.5 (0.12)	0.68 ± 0.20 (0.01)	0.56 ± 0.06 (0.08)
East Indian subcontinent	0.27 ± 0.42 (0.01)	0.005 ± 0.012 (0.001)	1.4 ± 0.53 (0.06)	2.7 ± 0.28 (0.07)	1.0 ± 0.25 (0.17)
Indian subcontinent	0.19 ± 0.14 (0.01)	0.03 ± 0.02 (0.004)	2.0 ± 1.7 (0.08)	1.8 ± 0.55 (0.04)	1.3 ± 0.57 (0.31)
Arabia	0.02 ± 0.03 (0.001)	<0.001	7.4 ± 2.9 (0.18)	1.3 ± 0.06 (0.03)	0.25 ± 1.1 (0.18)
Indian subcontinent-Arabia	0.06 ± 0.08 (0.001)	<0.001	6.1 ± 2.6 (0.08)	2.4 ± 0.53 (0.03)	0.92 ± 0.29 (0.10)
Arabian Sea-coastal India	0.06 ± 0.06 (0.001)	<0.001	2.7 ± 2.1 (0.08)	1.2 ± 0.54 (0.01)	0.68 ± 0.51 (0.10)

[a]Here μg C m^{-3} of OC × 1.6.

for other ocean regions. Mean concentrations ranged from 1.4 ± 0.53 μg m^{-3} for the EIndSub region to 10 ± 3.7 μg m^{-3} for the SHAtl region (Table 6). Mean concentrations for different air mass types over the northeast Atlantic during ACE 2 ranged from 4 to 10 μg m^{-3} [*Quinn et al*., 2000b] and for the central Atlantic during Aerosols99 ranged from 4 to 19 μg m^{-3} [*Quinn et al*., 2001]. The experimental average during ACE 1 conducted in the Southern Ocean region was 9.4 ± 5.5 μg m^{-3} [*Quinn et al*., 1998].

[61] In the supermicron size range, the measured NO_3^- was assumed to be associated with sea salt through the reaction of combustion-derived HNO_3 and sea salt [*Clegg and Brimblecombe*, 1985]. NO_3^- concentrations were low relative to sea salt in the SHAtl, SHIO, and NHIO regions. They were high in the continentally impacted regions being, on average, twice the sea-salt concentration in the EIndSub region, comparable to sea salt in the IndSub region, and 17 to 44% of the sea-salt concentration in the Arabia, Arabia/IndSub, and AS/CI regions.

[62] Sea-salt aerosol dominated the supermicron mass in all source regions (Figure 5). Mean mass fractions ranged from 55 ± 4.5% in the IndSub region to 97 ± 4.3% in the SHAtl region. Sea-salt aerosol made up the majority of the sub-10 μm aerosol mass in the SHAtl (95%), SHIO (91%), NHIO (72%), and Arabia (58%) regions. It made up 23% of the sub-10 μm mass in the EIndSub region, 27% in the IndSub region, 48% in the Arabia/IndSub region, and 34% in the AS/CI region.

4.2.3. IOM

[63] As explained in section 2.4, an inorganic oxidized material (IOM) component was constructed from the concentration of the major elements in soil and fly ash with a correction to the mass assuming that the elements were present in their normal oxidized form. This component most likely consists of fly ash with an intermittent soil dust contribution. Spectral absorption measurements of bulk aerosol collected on the *Ronald H. Brown* showed elevated absorption at the UV-blue wavelengths, an indicator of soil dust, only in the Arabia/IndSub and Arabia regions (D. Savoie, personal communication, 1999). During these periods, low-level trajectories were coming from Arabia to the ship.

[64] Submicron concentrations of IOM were less than 0.07 μg m^{-3} in the SHAtl, SHIO, and NHIO regions (Table 7). They were higher in the more continentally influenced source regions ranging from 0.42 μg m^{-3} in the AS/CI region to 1.7 μg m^{-3} in the IndSub region. The mean submicron mass fraction of IOM was highest in the Arabia region (21 ± 3.1%). In all other source regions the submicron mass fraction was less than 8.8%.

[65] Mean supermicron concentrations of IOM were less than 0.12 μg m^{-3} in the SHAtl and SHIO regions (Table 7). They ranged between 3.4 (NHIO) and 8 μg m^{-3} (Arabia/IndSub) for the other regions. Mean supermicron mass fractions were less than 1% in the SHAtl and SHIO regions and 14 ± 1.4% in the NHIO (Figure 5). For the more continentally influenced source regions values ranged from 23% (EIndSub) to 34% (AS/CI).

4.2.4. POM

[66] POM and BC concentrations and mass fractions are presented here to aid in the interpretation of the extinction due to these components. A more detailed discussion of these components for the INDOEX cruise can be found in the work of *Neusüss et al*. [2002]. Mean submicron POM concentrations were less than or equal to 0.16 μg m^{-3} for the SHAtl, SHIO, and NHIO (Table 5). Concentrations in the continentally influenced air mass source regions ranged from 0.42 ± 0.20 μg m^{-3} for the AS/CI region to 1.4 ± 0.08 μg m^{-3} for the EIndSub region. Mean submicron mass fractions for the marine source regions ranged from 2.1 ± 1.1% for NHIO to 10 ± 2.6% for SHAtl (Figure 4). Values for the continentally influenced source regions were near 5% for EIndSub, IndSub, IndSub/Arabia, and AS/CI. Highest values corresponded to the Arabia region (15 ± 4.0%).

[67] Mean supermicron POM concentrations were similar to the submicron values ranging from 0.14 to 0.56 μg m^{-3} for the marine regions and 0.25 to 1.3 μg m^{-3} for the continentally influenced regions (Table 6). The size distribution of POM depends on the processes by which it is incorporated into the aerosol particles. Its existence in the supermicron size range suggests that gas phase organics were adsorbed onto relatively large particles or it had a source in the ocean surface layer and was injected into the atmosphere in a manner similar to sea salt. Mean supermicron POM mass fractions were near 1 to 2% for the marine regions and <1 to 9% for the continentally influenced regions.

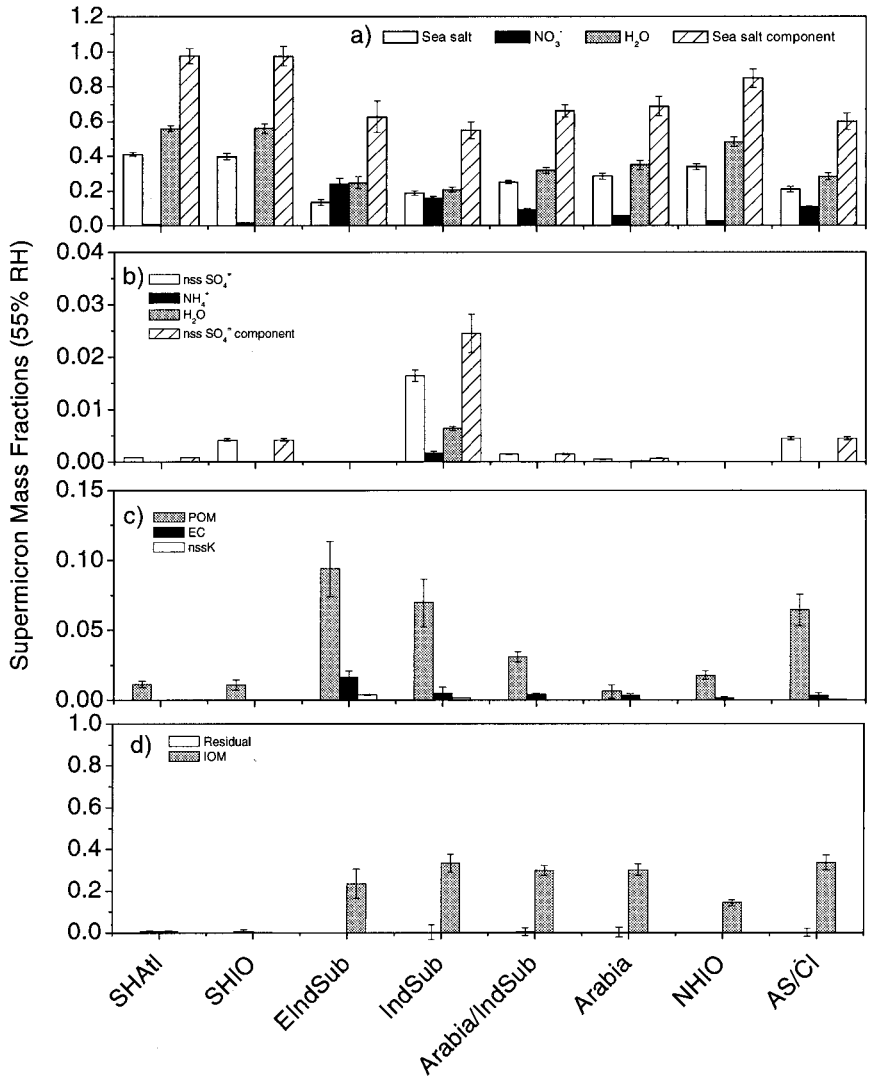

Figure 5. Regional mean supermicron mass fractions of the dominant chemical components at 55% RH. Error bars indicate the uncertainty at the 95% confidence level. The sea-salt component mass includes sea salt, nitrate, and water. The nss sulfate component includes nss $SO_4^=$, NH_4^+, and water. The number of samples available for the mass fraction calculation in each region was as follows: SHAtl 7, SHIO 5, EIndSub 1, IndSub 2, Arabia/IndSub 4, Arabia 2, NHIO 3, AS/CI 3.

4.2.5. BC and nss K^+

[68] Submicron BC concentrations were below the detection limit of 0.01 μg m^{-3} in the SHAtl and SHIO regions (Table 5). They were higher in the NHIO region (mean of 0.14 $\pm$ 0.05 μg m^{-3} with a range from 0.08 to 0.23 μg m^{-3}) indicating transport of anthropogenic aerosol from continental regions to the ITCZ region. Mean concentrations were relatively low in regions where low level air came from Arabia (0.08 $\pm$ 0.05 μg m^{-3} for the Arabia region and 0.54 $\pm$ 0.36 μg m^{-3} for the Arabia/IndSub region) or low-level air had not been in contact with land 6 days prior to being sampled on the ship (0.38 $\pm$ 0.12 μg m^{-3} for the AS/CI region). Mean concentrations were highest for regions where low level air came from the Indian subcontinent to the ship (1.8 $\pm$ 0.23 μg m^{-3} for the EIndSub region and 1.4 $\pm$ 0.06 μg m^{-3} for the IndSub region). These values exceed the range measured over the northeast Atlantic during ACE 2 (0.1 to 1.1 μg m^{-3} [*Novakov et al.*, 2000]) and the range inferred for the western Atlantic during TARFOX (up to 0.9μg m^{-3} [*Novakov et al.*, 1997].

[69] The submicron BC to TC mean ratio was smallest for the Arabia region (0.12 $\pm$ 0.13) and between 0.5 and 0.7 for all other source regions. Hence a relatively wide range of values were measured on the ship due to the expanse of the Indian Ocean and the variety of the air mass source regions impacting it. Mean ratios measured on three C130 flights at altitudes lower than 2 km ranged from 0.43 to 0.51 [*Novakov and Ramanathan*, 2001]. Submicron mean mass fractions of BC were below the detection limit for the SHAtl and SHIO regions (Figure 4), 2.7 $\pm$ 0.4% for the NHIO region, and between 1.5 (Arabia) and 7.5% (EIndSub) for the continentally influenced regions.

[70] Aerosol nss soluble K^+ is a by product of biomass burning and has been found to correlate well with BC concentrations [*Cachier et al.*, 1995]. As for BC, mean submicron nss

Table 7. Concentrations, Standard Deviations ($\pm 1\sigma$), and Absolute Uncertainties (95% Confidence Level, Shown in Parentheses) of the Mean of Aerosol Inorganic Oxidized Matter (IOM) and Residual Mass Concentrations for the Submicron ($D_{aero} < 1.1$ μm at 55% RH) and Supermicron ($1.1 < D_{aero} < 10$ μm at 55% RH) Aerosol for the Different Air Mass Regimes

	Submicron, $\mu g\ m^{-3}$		Supermicron, $\mu g\ m^{-3}$	
Air Mass Regime	IOM[a]	Residual[b]	IOM[a]	Residual[b]
SH Atlantic	0.06 ± 0.05 (0.02)	<0.01	0.12 ± 0.10 (0.08)	0.08 ± 0.04 (0.04)
SH Indian Ocean	0.07 ± 0.10 (0.02)	0.19 ± 0.14 (0.08)	0.02 ± 0.02 (0.004)	0.06 ± 0.05 (0.05)
NH Indian Ocean	0.07 ± 0.06 (0.04)	0.35 ± 0.49 (0.15)	3.4 ± 2.1 (0.29)	<0.01
East Indian subcontinent	1.6 (0.23)	<0.01	12 (1.5)	<0.01
Indian subcontinent	1.7 (0.18)	0.57 (0.78)	6.3 (0.60)	0.15 (0.73)
Arabia	1.1 (0.14)	<0.01	7.4 ± 1.8 (0.56)	0.04 ± 0.04 (0.56)
Arabia-Indian subcontinent	0.70 ± 0.50 (0.06)	0.61 ± 0.58 (0.25)	8.0 ± 2.7 (0.52)	0.14 ± 0.28 (0.52)
Arabian Sea-coastal India	0.42 ± 0.34 (0.08)	0.93 ± 0.65 (0.28)	4.4 ± 2.9 (0.38)	<0.01

[a]Based on [IOM] = 2.2[Al] + 2.49 [Si] + 1.63 [Ca] + 2.42 [Fe] + 1.94 [Ti] from *Malm et al*. [1994].
[b]Based on gravimetric mass less the sum of the chemically analyzed mass.

K^+ concentrations were highest in the EIndSub (0.58 ± 0.05 $\mu g\ m^{-3}$) and IndSub (0.44 ± 0.14 $\mu g\ m^{-3}$) regions. Submicron mean mass fractions were 2.2% or less in all source regions. Mean regional ratios of nss K^+ to BC ranged from 0.30 (IndSub and EIndSub) to 0.52 (AS/CI) and 0.61 (Arab/IndSub) in the continentally influenced regions. The mean ratio for the NHIO region was 0.66 ± 0.18. For comparison, a mean ratio of 0.52 ± 0.11 has been reported for biomass burning aerosol in Brazil [*Ferek et al*., 1998]. The range of values measured on the ship indicates a variable yet significant contribution of biomass burning aerosol to the Indian Ocean.

[71] Mean supermicron BC mass fractions were less than 2% in all source regions. Similarly, nss K^+ mean mass fractions were less than 0.5% in all source regions.

4.2.6. Residual

[72] The concentration of residual mass was calculated from the gravimetric mass minus the sum of the chemically analyzed species (ionic, POM, BC, and IOM). Mean submicron and supermicron concentrations are reported in Table 7. Submicron mean mass fractions ranged from less than the detection limit to 15%. Supermicron mean mass fractions ranged from less than the detection limit to 0.8%. The residual mass is most likely a result of inaccuracies in the estimate of the water associated with the aerosol at 55% RH, the selection of a constant POM factor of 1.6 for the entire experiment, and the assumption of the composition of the IOM component.

4.2.7. Other Chemical Components

[73] Other chemical components that were detected but that contributed less than one percent to the submicron mass were NO_3^- (presumably associated with NH_4^+) and MSA^-. MSA^- also was detected in the supermicron aerosol but made up <1% of the supermicron mass in all source regions.

4.3. Regional Optical Properties

4.3.1. Sub-1 μm to sub-10 μm Extinction Ratio

[74] Sub-1 μm and sub-10 μm scattering and absorption coefficients were measured as described in section 2.6. Extinction coefficients at 550 nm and 55% RH were derived from the sum of the STP- and angular corrected scattering coefficients and the absorption coefficients. Mean values and percentile information for the ratio of sub-1 μm to sub-10 μm extinction coefficients for the different air mass source regions are shown in Figure 6. Mean ratios were lowest in the marine regions south of the ITCZ (28 ± 7.4% for SHAtl, 40 ± 10% for SHIO, mean and 1σ standard deviation). The aerosol in these source regions was dominated by supermicron sea salt resulting in large extinction in the supermicron size range. The mean ratio was higher for the NHIO (60 ± 2.7%); supermicron mass concentrations were similar to those in the other marine regions but submicron nss sulfate aerosol concentrations also were higher. The mean ratio also was relatively low for the Arabia region (53 ± 4.3%) due to large concentrations of supermicron aerosol. On the basis of chemical analyses and spectral absorbances of filters collected in this region (D. Savoie, personal communication, 1999), the supermicron aerosol was composed of sea salt and soil dust.

[75] Mean sub-1 μm to sub-10 μm extinction ratios were comparable for the Arabia/IndSub (74 ± 7.7%) and AS/CI

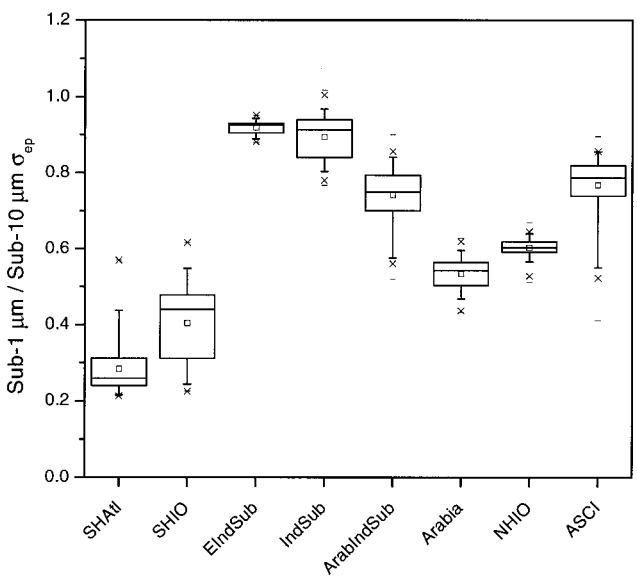

Figure 6. Mean regional ratios of sub-1 μm to sub-10 μm extinction at 550 nm and 55% RH. Extinction values are based on the sum of measured STP- and angular-corrected σ_{sp} from the nephelometer and measured STP-corrected σ_{ap} from the PSAP.

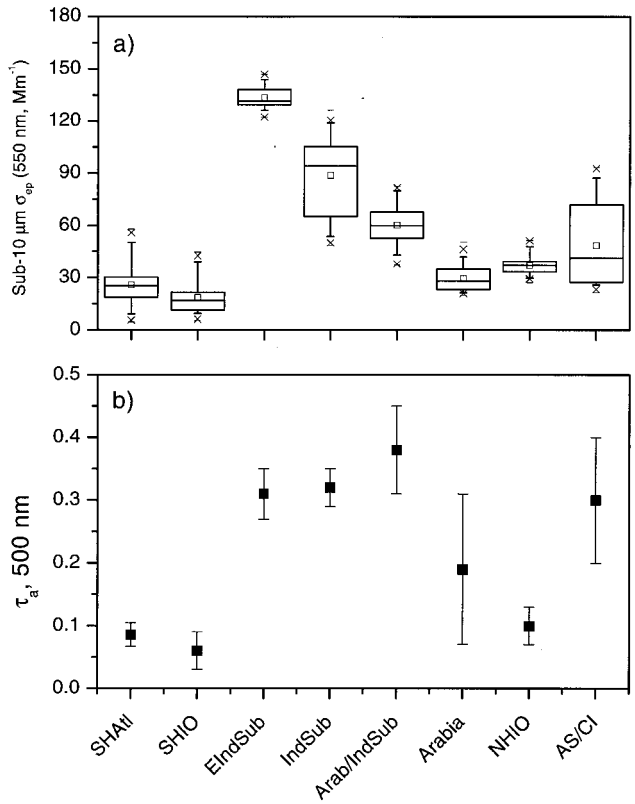

Figure 7. (a) Box plot of the sub-10 μm extinction coefficient (based on the sum of measured STP- and angular-corrected σ_{sp} from the nephelometer and measured STP-corrected σ_{ap} from the PSAP) at 550 nm and 55% RH for each air mass region. The horizontal lines in the box denote the 25th, 50th, and 75th percentile values. The error bars denote the 5th and 95th percentile values. The two symbols above and below the ends of the error bars indicate the 0th and 1st and the 99th and 100th percentile values. The open symbol in the box denotes the mean. (b) Mean and standard deviation (1σ) of aerosol optical depth at 500 nm for each air mass region.

(77 ± 8.7%) regions. Both regions had relatively high submicron mass concentrations composed of nss sulfate aerosol, POM, BC, and IOM. Submicron mass concentrations were about twice as high in the EIndSub and IndSub regions resulting in sub-1 μm to sub-10 μm extinction ratios of 92 ± 1.9% and 89 ± 6.1%. These source regions had the highest mass concentrations of submicron aerosol.

4.3.2. Aerosol Extinction and Backscattering Coefficients

[76] Mean values and percentile information for sub-10 μm aerosol extinction at 550 nm and 55 ± 5% RH for the different air mass source regions are shown in Figure 7a. Mean extinction coefficients were lowest for the SHAtl (26 ± 11 Mm^{-1}, mean and 1σ standard deviation) and SHIO (19 ± 10 Mm^{-1}) regions. Mean values were slightly higher for the NHIO (37 ± 5.2 Mm^{-1}). These extinction coefficients are comparable to those reported for other marine regions. Measured values of sub-10 μm extinction during ACE 2 in the northeast Atlantic averaged 22 Mm^{-1} and during ACE 1 in the Southern Ocean averaged 27 Mm^{-1} [*Quinn et al.*, 2000b, 1998]. Mean sub-10 μm extinction for the Arabia region was similar to the NHIO averaging 30 ± 6.9 Mm^{-1}. Air masses transported from Arabia to the ship did not contain the large concentrations of submicron nss sulfate aerosol, POM, and BC that those from the Indian subcontinent did. In addition, the accumulation mode surface mean diameter of the Arabia aerosol was smaller and the coarse mode surface mean diameter was larger relative to the Indian subcontinent aerosol (Table 3). Both factors result in a lower sub-10 μm extinction.

[77] Lower-level (500 m) trajectories for the AS/CI region indicated that the sampled air masses had not been over land for at least 6 days prior to reaching the ship. This region also had a relatively low mean sub-10 μm extinction of 48 ± 23 Mm^{-1} relative to the IndSub and EIndSub regions. Mean sub-10 μm extinction for the Arabia/IndSub region was higher (60 ± 11 Mm^{-1}) due to a larger submicron mass concentration perhaps resulting from mixing of Indian subcontinent aerosol into the marine boundary layer. Highest mean extinction coefficients corresponded to the two regions with lower-level flow from the Indian subcontinent, EIndSub (130 ± 5.8 Mm^{-1}) and IndSub (89 ± 22 Mm^{-1}). These are higher than mean values for western European air measured during ACE 2 (80 ± 21 Mm^{-1}) [*Quinn et al.*, 2000b] and within the range measured at altitudes lower than 300 m during TARFOX (24 to 200 Mm^{-1}) [*Hegg et al.*, 1997].

[78] Sub-10 μm mean backscatter coefficients showed the same trend as the extinction coefficients being highest for the EIndSub and IndSub regions and lowest for the marine and Arabia regions. Resulting mean sub-10 μm backscattered fractions were relatively constant spanning the limited range from 0.091 ± 0.004 to 0.11 ± 0.004. Sub-1 μm mean values ranged from 0.089 ± 0.008 to 0.11 ± 0.02.

4.3.3. Aerosol Angström Exponents

[79] Mean regional Angström exponents å for the 450 and 700 nm nephelometer wavelength pair derived from

$$\text{å} = -\frac{\log(\sigma_{sp}(\lambda_1)/_{sp}(\lambda_2))}{\log(\lambda_1/\lambda_2)} \quad (4)$$

are shown for the sub-10 μm aerosol in Figure 8a. Mean values were lowest for the marine regions, particularly those in the southern hemisphere where supermicron sea salt dominated the aerosol mass. Values were near 1.0 for the regions with low-level flow from Arabia and near 1.5 for regions with low-level flow from the Indian subcontinent.

4.3.4. Aerosol Absorption Coefficient and Single Scattering Albedo

[80] Mean sub-1 μm σ_{ap} were highest for the EIndSub (18 ± 1.3 Mm^{-1}) and IndSub (12 ± 4.4 Mm^{-1}) regions resulting from the relatively large concentrations of BC. For the majority of the sampling periods, absorption coefficients for the southern hemisphere marine regions, SHAtl and SHIO, were less than the detection limit of 0.34 Mm^{-1}. Mean values for the NHIO and Arabia regions were 2.4 ± 0.35 and 1.0 ± 0.20 Mm^{-1}, respectively. Mean values for the AS/CI and Arabia/IndSub regions were 5.0 ± 2.3 and 4.9 ± 1.8 Mm^{-1}, respectively.

[81] Single scattering albedo ω_o calculated as

$$\omega_o = \frac{\sigma_{sp}}{\sigma_{sp} + \sigma_{ap}} \quad (5)$$

is a measure of the relative magnitude of scattering and absorption by the aerosol. Here σ_{sp} is the nephelometer-measured scattering coefficient corrected for angular nonide-

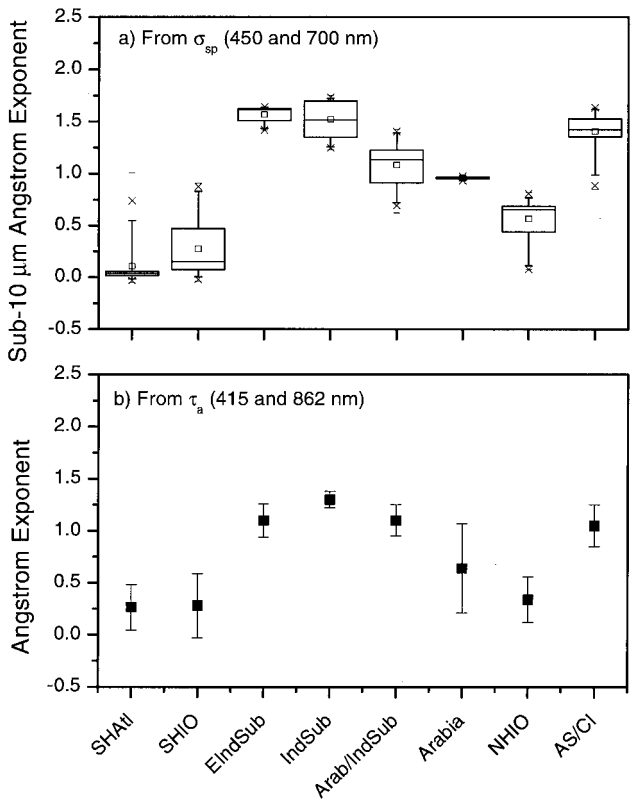

Figure 8. (a) Box plot of the Ångström Exponent (450 and 700 nm wavelength pair) derived from the STP- and angular-corrected σ_{sp} for sub-10 μm aerosol and 55% RH. Percentile information is as described in Figure 7 caption. (b) Mean and standard deviation (1σ) of the Ångström Exponent (415 and 862 nm wavelength pair) derived from the measured column aerosol optical depth for the different air mass regions.

alities as per equation (3), and σ_{ap} is the measured absorption coefficient corrected as per *Bond et al*. [1999]. Mean regional values of ω_o (550 nm) for sub-10 μm aerosol at 55% RH and sub-1 μm aerosol at 55% and 75% RH are listed in Table 8. Three levels of regional mean ω_o values are apparent. For sub-1 μm aerosol at 55% RH, mean values near one were observed in the southern hemisphere marine regions. Lower values were observed in the northern hemisphere marine region (0.89 ± 0.01) and in the regions with low-level flow from Arabia (0.93 ± 0.02 for Arabia and 0.89 ± 0.02 for Arabia/IndSub). Lowest mean values correspond to the regions exposed to low-level flow from the Indian subcontinent (0.85 ± 0.01 for EIndSub and 0.84 ± 0.01 for IndSub). Comparable mean values were observed in the AS/CI region (0.86 ± 0.01).

[82] Elevated absorption at the UV-blue wavelengths suggests that the aerosol collected in the regions with low-level flow from Arabia contained soil dust. In addition, BC concentrations in these regions were low compared to the regions with low-level flow from India. The mass fraction of IOM in the Arabia and Arabia/IndSub regions was equivalent to or larger than the BC mass fraction in the EIndSub and IndSub regions. The equivalent IOM and BC mass fractions but higher ω_o in the Arabia and Arabia/IndSub regions suggests that the soil dust component had a lower mass absorption efficiency at 550 nm than did BC in the EIndSub and IndSub regions.

4.4. Regional Extinction Due to Individual Aerosol Chemical Components

[83] The fraction of the measured extinction (scattering plus absorption) due to the major aerosol chemical components was calculated at 55% RH and 550 nm using the method described in section 3.2. The major components considered are sea-salt aerosol which includes supermicron NO_3^- and water calculated to be associated with sea salt at 55% RH; nss sulfate aerosol which includes nss $SO_4^=$, NH_4^+, and water at 55% RH; a combustion component composed of BC, KNO_3, and K_2SO_4; POM; and IOM. For these calculations, the IOM and residual mass were combined into one component. Results are shown for the submicron, supermicron, and sub-10 μm aerosol in Figures 9, 10, and 11. In general, the trend in extinction fractions for each of the chemical components follows the trend in their mass fractions.

4.4.1. Non-Sea-Salt Sulfate Aerosol

[84] The contribution of nss sulfate aerosol to submicron extinction ranged from 19 to 55% (Figure 9). This range is higher than that estimated for submicron nss sulfate extinction over the Atlantic Ocean during the Aerosols99 cruise (up to 25%) [*Quinn et al*., 2000a]. Smallest contributions were in the southern hemisphere marine regions (SHAtl = 19 ± 6.3% and SHIO = 29 ± 14%, mean and 1σ standard deviation) due to relatively high extinction by submicron sea-salt aerosol. Mean

Table 8. Single Scattering Albedo ω_o at 550 nm for Sub- 10 and Sub- 1 μm Aerosol at the Measurement Relative Humidity of 55% and at 75%[a]

	ω_o, 550 nm		
Air Mass Region	55% RH, sub-10 μm	55% RH, sub-1 μm	75% RH[b], sub-1 μm
SH Atlantic[c]	1.0 ± 0.02	1.0 ± 0.02	1.0 ± 0.02
SH Indian Ocean[c]	1.0 ± 0.02	1.0 ± 0.04	1.0 ± 0.04
NH Indian Ocean	0.95 ± 0.02	0.89 ± 0.01	0.91 ± 0.01
East Indian subcontinent	0.86 ± 0.01	0.85 ± 0.01	0.88 ± 0.01
Indian subcontinent	0.86 ± 0.02	0.84 ± 0.01	0.87 ± 0.01
Arabia	0.96 ± 0.01	0.93 ± 0.02	0.94 ± 0.02
Arabia/Indian subcontinent	0.92 ± 0.02	0.89 ± 0.02	0.91 ± 0.02
Arabian-Sea/coastal India	0.88 ± 0.02	0.86 ± 0.01	0.89 ± 0.91

[a]Values are reported at STP.
[b]Here σ_{sp} was from the measurement RH of 55% to 75% using measured f(RH) curves at Kaashidoo Climate Observatory during the INDOEX 1999 intensive [*Ramanathan et al*., 2001].
[c]Upper bound; σ_{ap} values less than the detection limit of 0.34 Mm^{-1} were considered to be zero.

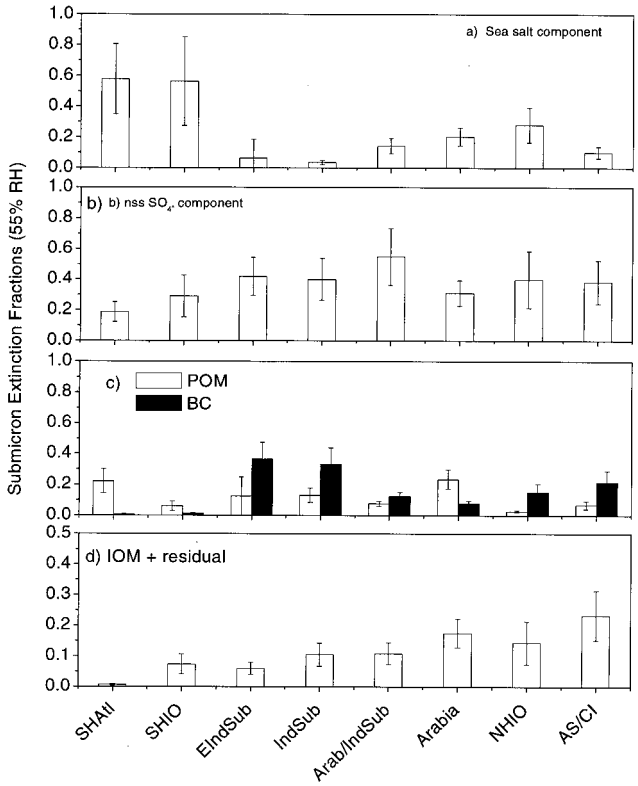

Figure 9. Mean regional fractional contribution of the submicron aerosol chemical components to extinction (scattering and absorption). Extinction fractions are reported at 55% RH and 550 nm. Error bars indicate the 1σ standard deviation of the mean.

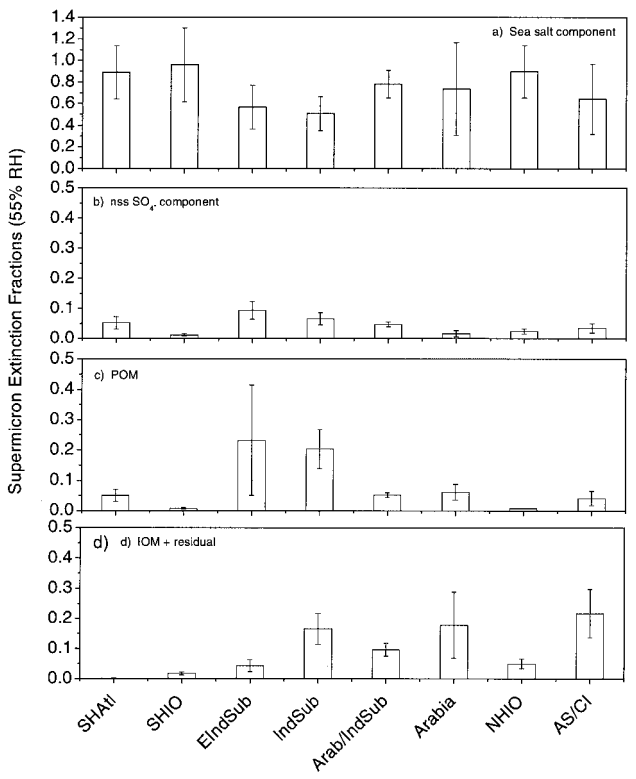

Figure 10. Mean regional fractional contribution of the supermicron aerosol chemical components to extinction (scattering and absorption). Extinction fractions are reported at 55% RH and 550 nm. Error bars indicate the 1σ standard deviation of the mean.

sulfate extinction in the northern hemisphere marine region (NHIO) was higher (40 ± 18%) due to lower submicron sea-salt concentrations and higher nss sulfate concentrations. The extinction fraction of sulfate aerosol was relatively low in the Arabia region (31 ± 8.2%) due to significant extinction by several components (sea salt, sulfate, IOM, and POM). The other region impacted by lower-level flow from Arabia, Arabia/IndSub, had a higher mean submicron extinction fraction of 55 ± 19% due to higher concentrations of sulfate and lower concentrations of POM and IOM. Submicron sulfate extinction fractions for the IndSub and EIndSub regions were 40 ± 14% and 42 ± 12%, respectively. Mean extinction in the AS/CI region was 38 ± 14%. Nss sulfate aerosol contributed less than 9% to supermicron extinction in all regions (Figure 10) and between 9% (SHAtl) and 46% (EIndSub) to the sub-10 μm extinction (Figure 11).

4.4.2. Sea-Salt Aerosol

[85] The contribution of sea salt aerosol to submicron extinction was highest in the southern hemisphere marine regions (SHAtl = 58 ± 23%, SHIO = 56 ± 29%) and relatively high in the northern hemisphere marine region of NHIO (28 ± 11%). For the more continentally influenced regions, extinction fractions ranged from around 3 to 6% (IndSub and EIndSub) to 20% (Arabia). The sea-salt extinction fractions in the INDOEX continentally influenced regions are low compared with those reported for regions of the Atlantic impacted by continental emissions from North America (36%) and biomass burning (29%) and dust (67%) emissions from Africa [*Quinn et al.*, 2001]. The difference is a result of higher concentrations of non-sea-salt chemical components rather than lower sea-salt concentrations.

[86] The sea-salt aerosol contribution to supermicron extinction ranged from 51% (IndSub) to 97% (SHAtl). The dominance by sea salt (even though IOM concentrations were comparable in some regions) is a result of its propensity for water uptake with increasing RH and its reluctance to release water with decreasing RH. As the relative humidity decreases from greater than 70% to 55%, sea salt retains water to the extent that the wet particle mass is twice the drier mass [*Tang et al.*, 1997]. Contribution of sea salt to sub-10 μm extinction ranged from 7 to 83%. This range is lower than that estimated for regions of the Atlantic (47 to 93%) [*Quinn et al.*, 2001] indicating the importance of non-sea-salt chemical components in determining the aerosol radiative forcing in the continentally influenced INDOEX air masses.

4.4.3. IOM

[87] For the purpose of the extinction calculations, the IOM and residual mass were combined. Hence the extinction fractions reported for IOM are based on both the IOM and the residual mass. The fraction of submicron extinction due to IOM was less than 1% in the SHAtl region. Mean submicron extinction due to IOM in the SHIO region was 7.4 ± 3.3% but was primarily due to residual mass. The mean extinction fraction in the NHIO region was 14 ± 7.0% and also was primarily due to residual mass. Mean submicron IOM extinction fractions were relatively low and comparable for the EIndSub

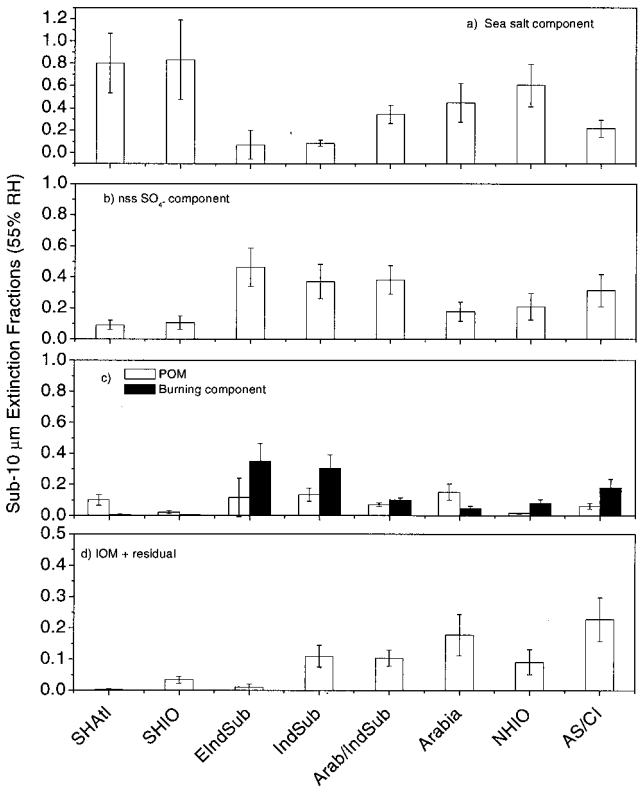

Figure 11. Mean regional fractional contribution of the sub-10 μm aerosol chemical components to extinction (scattering and absorption). Extinction fractions are reported at 55% RH and 550 nm. Error bars indicate the 1σ standard deviation of the mean.

(5.9 ± 14%), IndSub (10 ± 3.8%), and Arabia/IndSub (11 ± 3.5%) regions. A portion of the extinction in the latter two regions was due to residual mass. Values were highest for the Arabia (17 ± 4.7%) and AS/CI (23 ± 8.1%) regions with a portion of the extinction in the AS/CI region due to residual mass.

[88] In the supermicron size range, extinction estimates for the IOM plus residual component are due solely to IOM because of the low residual mass concentrations. The contribution of IOM to supermicron extinction averaged less than 5% for the southern and northern hemisphere marine regions. The mean value also was less than 5% for the EIndSub region due to significant mass fractions of sea salt and POM and the higher mass extinction efficiencies of these two components (see Table 8). Mean values for the other continentally-influenced regions ranged from 9.6 ± 2.0% for the Arabia/IndSub region to 22 ± 8.1% for the AS/CI region. The contribution of IOM to sub- 10 μm extinction ranged from less than 1% to 23%.

4.4.4. POM

[89] The mean POM submicron extinction fraction was variable and seemingly independent of air mass type. It was relatively high in both marine and continentally-influenced air mass regions (22 ± 7.9% in the SHAtl region and 23 ± 6.3% in the Arabia region). Mean values also were low in both marine and continentally influenced air mass regions (2.8 ± 0.1% in the NHIO region and 6.8 ± 2.6% in the AS/CI region). The variability in the submicron POM extinction fractions is similar to what was found for marine and continentally influenced regions of the Atlantic. During the Aerosols99 cruise, mean extinction fractions ranged from less than 1% for air masses influence by African dust and 18% for northern hemisphere marine air masses [*Quinn et al*., 2002].

[90] Mean supermicron extinction fractions were consistently low (<6%) in all regions except the EIndSub and IndSub regions were they reached values of 23 ± 18% and 20 ± 6.4%, respectively. Mean sub- 10 μm extinction fractions of POM ranged from 1.6% (NHIO) to 15% (Arabia).

4.4.5. BC and nss K^+ (Burning Component)

[91] BC and nss K^+ associated with $SO_4^=$ and NO_3^- were grouped into a burning component. Extinction due to the entire component was then calculated. This component contributed less than 1% to the submicron extinction in the southern hemisphere marine regions. Mean submicron extinction for the NHIO was higher (15 ± 5.5%) indicating transport of continental aerosol to the ITCZ. Mean submicron extinction was relatively low for the two regions with lower-level flow from Arabia (7.7 ± 1.8% for Arabia and 12 ± 2.5% for Arabia/IndSub). It was 21 ± 7.5% for the AS/CI region and highest for the two regions with lower-level flow from the Indian subcontinent (36 ± 11% for EIndSub and 33 ± 11% for IndSub). Contributions to supermicron extinction were negligible.

[92] The substantial contributions of BC to extinction in the Indian subcontinent air masses is similar to what was observed during the 1998 INDOEX IFP. Model calculations using data collected at the Kaashidhoo Climate Observatory estimated that 11% of the τ_a at ambient RH was due to soot [*Satheesh et al*., 1999]. Similar results were obtained for the 1999 INDOEX IFP [*Ramanathan et al*., 2001].

4.5. Mass Extinction Efficiencies of the Individual Aerosol Chemical Components

4.5.1. Comparison of Two Methods

[93] Mass extinction efficiencies $\alpha_{ep,j}$ of individual chemical components are defined as

$$\alpha_{ep,j} = \frac{\sigma_{ep,j}}{m_j}, \tag{6}$$

where $\sigma_{ep,j}$ is the extinction coefficient for component j and m_j is the mass of component j. An empirical and a calculational approach were used to calculate $\alpha_{ep,j}$ for the sub-10 μm size range (at 55% RH and 550 nm) to check for consistency between the methods. A thorough discussion of the advantages and disadvantages of each approach can be found in the work of *Charlson et al*. [1999]. The empirical approach used a multiple linear regression of the mass concentration of the major chemical components against the extinction coefficient for the whole aerosol. The following equation was used to obtain weighted averages of the extinction efficiencies:

$$\sigma_{ep} = \alpha_{ep,\mathrm{seasalt}}\mathrm{m}_{\mathrm{seasalt}} + \alpha_{ep,\mathrm{SO4,ion}}\mathrm{m}_{\mathrm{SO4,ion}} + \alpha_{ep,\mathrm{IOM}}\mathrm{m}_{\mathrm{IOM}} + \alpha_{ep,\mathrm{POM}}\mathrm{m}_{\mathrm{POM}} + \alpha_{ep,\mathrm{BC}}\mathrm{m}_{\mathrm{BC}}, \tag{7}$$

where σ_{ep} is the sum of the measured sub-10 μm σ_{sp} and σ_{ap} and the mass concentrations are a sum of the measured submicron and supermicron concentrations for each component. The IOM component consists of IOM and residual mass. Residual mass made up less than 4% of the sub-10 μm mass in all source regions. The entire data set was used rather than de-

Table 9. Comparison of Mass Extinction Efficiencies Derived From Mie Calculations (Calculated) and From a Multiple Linear Regression (Empirical) at 550 nm[a]

	Empirical[b]		Calculated		Previously Reported
Component	Coefficient	Standard Error	Mean	Range	Range
Sea salt	1.7	0.4	1.6	0.98–3.3	0.61–2.1[c]
NSS $SO_4^=$ ion	2.0	0.78	4.9	2.0–6.6	4.2–7.5[c]
IOM plus residual	0.51	4.3	1.5	0.56–2.7	1.07[d]
					0.73–0.79[e]
POM	1.6	4.3	4.1	1.2–5.8	2.6–3.6[f]
BC[g]	8.5[h]	1.3	8.8	1.6–14	

[a]Values are for the size range $D_{aero} < 10$ μm (at 55% RH) and are means over the entire experiment. Units are in m^2 g^{-1}.
[b]Based on equation (6); $r^2 = 0.93$; number of samples equal to 41.
[c]From a regression similar to equation (6) where y is the measured absorption coefficient. Only samples with measurable black carbon were included; $r^2 = 0.93$; number of samples equal to 22.
[d]*Chiapello et al*. [1999]; Sal Island, 670 nm.
[e]*Li et al*. [1996]; Barbados.
[f]*Patterson and McMahon* [1984]; *Tangren* [1982]; smoke particles in the smoldering phase.
[g]Mass absorption efficiency.
[h]*Quinn et al*. [1996]; Pacific Ocean.

riving regional averages because of the small number of samples collected in some regions. The calculational approach, based on the Mie calculation described in section 3.2, was used to calculate $\alpha_{ep,j}$ for the sub-10 μm size range for comparison to the empirical approach.

[94] Mean values from the two methods are compared in Table 9. For all components except the IOM, $\alpha_{ep,j}$ calculated from the multiple linear regression falls within the range of values derived from the Mie calculation. The value of $\alpha_{ep,IOM}$ from the regression is about 10% below the range from the Mie calculation but has a large standard error. The agreement between the two independent methods confirms the internal consistency in the data set and indicates that the derived parameters are accurate within experimental uncertainty.

4.5.2. Submicron and Supermicron Component Mass Extinction Efficiencies

[95] The calculational method also was used to calculate $\alpha_{ep,j}$ at 550 nm for the submicron and supermicron size ranges for the different air mass source regions. In these calculations, sea salt and NO_3^- in the supermicron size range were combined to form the sea-salt component, and nss $SO_4^=$ was combined with NH_4^+ to form the sulfate aerosol component. Both of these components also included the mass of water calculated to be associated with them at 55% RH. The value of $\alpha_{ep,j}$ also was calculated for the nss sulfate ion such that $\sigma_{ep,j}$ is the scattering due to sulfate aerosol (nss $SO_4^=$, NH_4^+, and water at 55% RH) and m_j is the mass of the nss $SO_4^=$ ion. The value of $\alpha_{ep,j}$ for the nss $SO_4^=$ ion is a useful quantity as chemical transport models predict the ion concentration or column burden of sulfate rather than the sulfate aerosol concentration [e.g., *Langner and Rodhe*, 1991]. Mean values are reported in Table 10 for the different air mass source regions.

[96] Mean mass extinction efficiencies of submicron sea salt ranged from 5.1 to 6.0 m^2 g^{-1}. Supermicron values ranged from 1.0 to 1.2 m^2 g^{-1}. Both sets of values compare well with those estimated for latitude bands of the Atlantic during the Aerosols99 Cruise. For the Atlantic, mean submicron values ranged from 5.4 to 7.8 m^2 g^{-1}, and supermicron values ranged from 0.9 to 1.3 m^2 g^{-1} for the aerosol at 55% RH [*Quinn et al*., 2002].

[97] Mean $\alpha_{ep,j}$ for submicron nss $SO_4^=$ aerosol ranged from 2.9 to 5.3 m^2 g^{-1} and for submicron nss $SO_4^=$ from 3.5 to 6.3 m^2 g^{-1}. These values also are comparable to those reported for latitude bands of the Atlantic (2.0 to 3.8 m^2 g^{-1} for sulfate aerosol and 2.5 to 5.8 m^2 g^{-1} for the sulfate ion). In addition, they fall within the theoretical range of low RH sulfate scattering efficiencies predicted by *Charlson et al*. [1999].

[98] Mean mass extinction efficiencies for submicron IOM ranged from 3.0 to 4.3 m^2 g^{-1}. Supermicron values ranged from 0.5 to 1.4 m^2 g^{-1}. These values are similar to those estimated for African dust that had been transported to the central Atlantic (3.5 m^2 g^{-1} for the submicron size range and 0.5 m^2 g^{-1} for the supermicron size range) [*Quinn et al*., 2001].

[99] Mean submicron POM mass extinction efficiencies ranged from 4.4 to 7.6 m^2 g^{-1} over all source regions. Supermicron values ranged from 2.8 to 5.5 m^2 g^{-1}. Because of the lack of information about the hygroscopicity of the sampled organic matter, no water was associated with the POM. By assuming that the water uptake by POM is similar to that of sulfate aerosol, *Liousse et al*. [1996] calculated an increase in $\alpha_{ep,j}$ from 4 for a dry aerosol to 6.8 m^2 g^{-1} for an aerosol at 80% RH due to an increase in particle size. The competing effect of lowering the refractive index must also be considered, however. Mean submicron mass extinction efficiencies for the burning component (BC plus submicron KNO_3 and K_2SO_4) ranged from 1.2 to 5.8 m^2 g^{-1}. Mean submicron mass absorption efficiencies for the burning component ranged from 9 to 15 m^2 g^{-1}.

4.6. Aerosol Optical Depth

[100] Lidar measurements made on the *Ronald H. Brown* indicated the presence of a single aerosol layer in the southern hemisphere marine regions which was embedded within the marine boundary layer (MBL) and reached up to 3 km [*Welton et al*., 2002]. No lidar measurements were made during the time period corresponding to the NHIO region. However, both 500 and 2500 m trajectories indicate that the sampled air had been over the northern hemisphere Indian Ocean for several days prior to being sampled (Table 1). In the northern hemisphere continentally influenced regions, an upper layer (UL) of aerosol was present between altitudes of 1 to 3 or 4 km.

[101] On the basis of trajectories, lidar profiles of aerosol backscatter, and vertical profiles of temperature and RH, sev-

Table 10. Mean and Standard Deviation (1σ) of the Mass Extinction Efficiencies of the Major Chemical Components in Each Air Mass Region[a]

	Sea Salt[b]		NSS Sulfate Ion[c]		NSS Sulfate Aerosol[d]		IOM Plus Residual		POM		BC and nss K[e]		Total Aerosol	
Region	mean	s.d.	mean	s.d.	mean	s.d.	mean	s.d.	mean	s.d.	mean	s.d.	mean	s.d.
							Submicron, $m^2\ g^{-1}$							
SH Atlantic	5.1	1.3	3.5	1.5	2.9	0.5	3.0	0.4	4.4	0.8	1.2	0.2	4.2	0.9
SH Indian Ocean	5.3	1.5	4.1	2.2	3.4	0.9	3.5	0.5	4.8	0.9	2.7	0.7	4.4	1.2
NH Indian Ocean	5.7	1.8	5.1	2.5	4.0	1.0	3.6	1.1	6.6	0.4	5.2	0.4	4.5	1.2
East Indian subcontinent	5.7	0.1	6.3	0.1	5.3	0.1	4.3	0.1	7.6	0.1	5.8	0.01	5.6	0.1
Indian subcontinent	5.3	1.2	5.7	2.1	4.4	0.9	3.3	0.7	6.7	1.4	5.8	0.1	4.8	0.9
Arabia	5.3	1.1	4.2	1.2	3.2	0.4	3.1	0.6	5.4	0.8	4.7	0.1	4.0	0.6
Arabia-Indian subcontinent	5.9	1.2	5.4	1.8	4.2	0.6	3.2	0.4	6.7	1.4	4.5	0.3	4.4	0.7
Arabian Sea coastal India	6.0	1.5	5.3	2.1	4.1	0.8	3.3	0.7	6.1	1.3	5.6	0.5	4.4	0.9
							Supermicron, $m^2\ g^{-1}$							
SH Atlantic	1.0	0.1					1.4	0.1	2.8	0.5			1.3	0.2
SH Indian Ocean	1.1	0.3					0.7	0.1	3.6	0.7			1.4	0.3
NH Indian Ocean	1.0	0.1					0.8	0.1	3.7	0.2			1.7	0.3
East Indian subcontinent	1.0	0.1	3.4	0.4	2.9	0.1	0.6	0.1	5.5	0.1			4.7	0.05
Indian subcontinent	1.1	0.2	4.1	2.8	3.5	0.6	0.6	0.1	4.9	0.9			3.7	0.6
Arabia	1.0	0.3	4.5	1.4	4.3	1.9	0.5	0.2	3.8	0.6			1.5	0.4
Arabia Indian subcontinent	1.1	0.1	3.7	0.2	4.1	0.6	0.7	0.04	3.7	0.4			2.3	0.2
Arabian Sea coastal India	1.2	0.4					0.7	0.2	4.6	0.8			2.7	0.5

[a]Integral values are reported at 55% RH for the submicron ($D_{aero} < 1.1\ \mu m$) and supermicron ($1.1 < D_{aero} < 10\ \mu m$) size ranges. Values are based on a Mie calculation at 550 nm. Units are in $m^2\ g^{-1}$.
[b]Includes NO_3 and water at 55% RH.
[c]Includes scattering due to nss $SO_4^=$, NH_4^+, and water at 55% and mass due to nss $SO_4^=$ ion.
[d]Includes scattering due to nss $SO_4^=$, NH_4^+, and water at 55% and mass due to nss $SO_4^=$, NH_4^+, and water at 55% RH.
[e]Nss K^+ with associated $SO_4^=$ and NO_3^-.

eral well-defined column aerosol situations become apparent [*Welton et al*., 2002]. These situations include (1) regions where there was a single aerosol layer confined to the MBL (SHAtl and SHIO), (2) regions where the MBL aerosol and the UL aerosol originated from the same or different source regions and were well mixed in the atmospheric column (EIndSub, IndSub, and portions of Arabia/IndSub, Arabia, and AS/CI), and (3) regions where the MBL aerosol and the UL aerosol originated from the same or different source regions and were not well mixed in the atmospheric column (portions of Arab/IndSub, Arabia, and AS/CI). Relationships between surface extinction and column extinction are expected to vary for these different situations.

[102] Mean regional τ_a are compared to surface extinction coefficients derived from measured σ_{sp} and σ_{ap} in Figure 7. As for surface extinction, relatively low τ_a were measured in the southern hemisphere marine regions (0.08 ± 0.02 for SHAtl and 0.06 ± 0.03 for SHIO). The mean value was slightly higher in the northern hemisphere marine region (0.10 ± 0.03 for NHIO). Also similar to surface extinction, relatively high τ_a were observed in the EIndSub (0.31 ± 0.04) and IndSub (0.32 ± 0.03) regions. For the rest of the source regions there is a departure in the pattern of τ_a from the pattern observed in surface extinction. Mean τ_a for the Arabia/IndSub (0.38 ± 0.07), Arabia (0.19 ± 0.12), and AS/CI region (0.30 ± 0.10) regions were higher than what would be expected based on the surface extinction values.

[103] The high variability in τ_a during the Arabia and AS/CI regions was a result of changing source regions for the MBL and/or UL aerosol. During a portion of the time period of the AS/CI region, trajectory analysis shows that the MBL aerosol originated from the AS/CI region and the UL aerosol originated from the Indian subcontinent. Values of τ_a during this period range from 0.37 to 0.54. Then a transition period occurred where the transport path of the MBL aerosol to the ship moved away from the Indian coast and the UL aerosol spent less time over India before reaching the ship. Values of τ_a during this period ranged from 0.25 to 0.29 with an outlier of 0.55. On the basis of vertical profiles of RH, at the end of the period, the surface moist layer was mixed up to a height of 8 km. The 500 and 2500 m trajectories both indicated flow from the AS/CI to the ship. Values of τ_a ranged from 0.18 to 0.25. For the Arabia region there were two distinct τ_a ranges corresponding to different source regions of the UL aerosol. Values of τ_a ranged from 0.06 to 0.17 when UL aerosol originated over Arabia and from 0.29 to 0.41 when the UL aerosol originated over India.

[104] Values of surface extinction and τ_a were compared more rigorously in a linear regression of individual data points. The regression reveals two distinct groups of data (Figure 12). All of the data from the marine regions (SHAtl, SHIO, and NHIO), EIndSub, and IndSub, and a portion of the data from the Arabia/IndSub, Arabia, and AS/CI regions fall along a regression line with a coefficient of determination, r^2, of 0.83 (as indicated by solid symbols in Figure 12). These data fall into the first and second situations described above, i.e., either a single aerosol layer was present (SHAtl, SHIO, and NHIO) or the MBL and UL aerosols were well mixed (EIndSub,

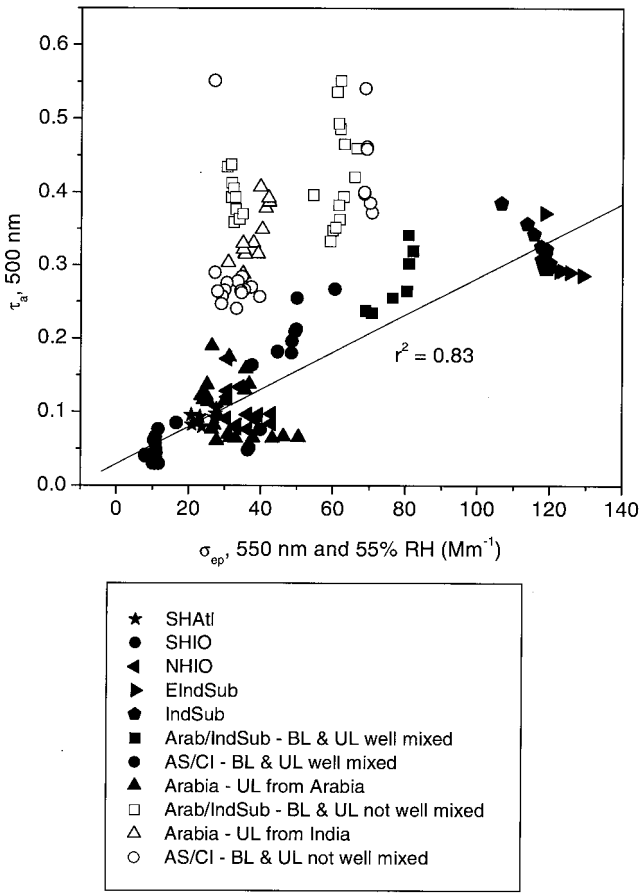

Figure 12. Linear regression of measured τ_a (500 nm) against surface extinction ($\sigma_{sp} + \sigma_{ap}$ at 550 nm and 55% RH). The line represents the linear fit for all data (solid symbols) collected when there was a single aerosol layer in the MBL, when MBL and UL aerosols were well mixed, or when the MBL and UL aerosol originate from similar source regions.

IndSub, and portions of Arabia/IndSub and AS/CI). An exception to this was the Arabia region during periods when the MBL and UL aerosols were not well mixed but both came from the same source region (Arabia). Shown in open symbols in Figure 12 are data which fit into the third situation described above, i.e., the MBL and UL aerosol were not well mixed (portions of Arab/IndSub and AS/CI). In addition, these data include periods from the Arabia region when the MBL and UL aerosols were not well mixed and came from different source regions (MBL from Arabia and UL from India). On the basis of this analysis, trends in surface extinction follow those of column extinction when there is a single aerosol layer in the MBL, when MBL and UL aerosols are well mixed, and when the MBL and UL aerosol originate from similar source regions.

[105] Also apparent in Figure 12 is the absence of a correlation in surface and column extinction within air mass regions but a significant correlation between air mass regions when vertically decoupled cases are excluded. This result implies that distinct air mass types that contain different aerosol mixtures tend to have similar vertical aerosol distributions when the MBL and UL aerosol is well mixed. Lidar observations on board the ship confirmed that distinct regions with well mixed aerosol layers had similar vertical distributions even though the magnitude of the extinction in each region varied due to different aerosol mixtures and sources [*Welton et al.*, 2000]. In these regions the inversion at the top of the MBL was not as strong (based on altitude gradients of RH) as in regions with decoupled layers. In addition, there was an absence of a significant trade wind inversion above the MBL.

[106] A similar analysis was performed on the Ångström exponents derived from the surface scattering and τ_a measurements. A comparison of mean regional values is shown in Figure 8. The general trend is similar for the surface and column values. Relatively low å were observed in marine regions where there are high concentrations of supermicron sea-salt aerosol, and high values were observed in continentally influenced regions where concentrations of submicron aerosol were high. The column mean regional values are lower than the surface values, however, most likely as a result of the difference in wavelength pairs. A linear regression of the individual data points is shown in Figure 13. A regression of all data points results in an r^2 of 0.43. If only the solid symbols are included (representing data derived from periods of a single aerosol layer, when the MBL and UL aerosol were well mixed, and when the MBL and UL aerosol originated from similar sources) r^2 equal 0.70. To lessen differences due to the choice of wavelength pairs, the Microtops å calculated for the 440/675 wavelength pair also is shown. In this case, $r^2 = 0.67$. The relationship between surface and column å is not as apparent as between surface and column extinction.

[107] UL aerosol properties, including the å, were measured onboard the C130 [*Sheridan et al.*, 2002]. Comparing these data to those measured on the ship is difficult, however, since the plane and the ship were rarely in the same vicinity experiencing similar MBL and UL transport patterns. In addition, the aircraft å are for the sub-1μm aerosol, while the shipboard values in Figures 8 and 13 are for sub-10 μm aerosol (a more appropriate size range for the comparison to column τ_a and å). This difference in size ranges does not limit the utility of ship/aircraft comparisons since, for many of the air mass source regions, submicron aerosol dominated extinction (Figure 6). A regression of surface sub-1μm å against surface sub-10μm å over all air mass source regions results in an r^2 value of 0.96.

[108] On the basis of C130 flights over the northern Indian Ocean (defined as latitudes greater than 5°N), the å decreased with altitude. Mean values for 0 to 1 km, 1 to 3 km, and 3 to 5 km were 1.99 ± 0.31, 1.83 ± 0.52, and 1.78 ± 0.85, respectively [*Sheridan et al.*, 2002]. When the northern hemisphere regions are sorted by trajectory, the trend in å with altitude is not as apparent, however. For example, in the six instances where the C130 sampled MBL air from AS/CI and UL air (1 to 4 km) from India (a transport pattern often encountered by the ship), there were flights when the mean UL level leg å was greater than, equal to, or less than the MBL level leg å. Variability of the Ångström Exponent within an air mass source region appears to preclude a well-defined relationship between surface and column values.

5. Conclusions

[109] Measurements made on board the R-V *Ronald H. Brown* during the 1999 INDOEX IFP indicated a large degree of variability in aerosol chemical and optical properties in the marine boundary layer over the Indian Ocean during the winter monsoon season. This variability is due to the wide range of

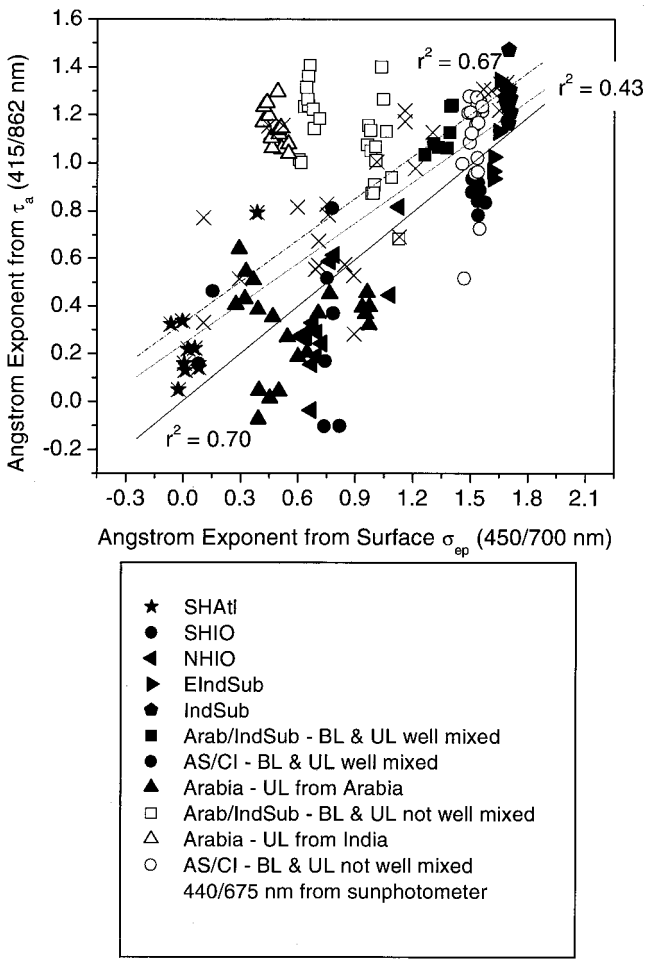

Figure 13. Linear regression of the Ångström exponent derived from τ_a (415 and 862 nm) against the Ångström exponent derived from surface measured σ_{sp} (450 and 700 nm). The dotted line represents the linear fit for all data. The solid line represents the linear fit for all data (solid symbols) collected when there was a single aerosol layer in the MBL, when MBL and UL aerosols were well mixed, or when the MBL and UL aerosol originate from similar source regions. Black crosses show the regression of the surface Ångström exponent versus the Ångström exponent derived from the Microtops sunphotometer at 440 and 675 nm. The regression for this relationship is indicated by the dashed line.

aerosol sources that impact the region and to changing transport pathways from the Indian subcontinent and nearby nations to the marine atmosphere. The southern hemisphere Indian Ocean was relatively uninfluenced by continental sources. Aerosol chemical composition, scattering and absorption coefficients, and optical depth for this region were similar to what has been reported for remote regions of the Pacific and Atlantic Oceans. Sea salt dominated both the sub-1 μm and the sub-10 μm extinction by aerosol particles. Compared to the southern hemisphere, northern hemisphere marine regions, which include the ITCZ, had elevated black carbon and nss sulfate aerosol concentrations as well as lower single scattering albedo values indicating the transport of continental aerosol as far south as the ITCZ. Nss sulfate aerosol dominated the sub-1 μm extinction, while sea salt dominated the sub-10 μm extinction.

[110] Simultaneous transport of low-level (500 m) and upper-level (2500 m) air masses from Arabia to the Indian Ocean resulted in higher concentrations of submicron nss sulfate aerosol, particulate organic matter, black carbon, and inorganic oxidized material (IOM). Yet marine boundary layer extinction was low (compared with regions influenced by the Indian subcontinent) due to the relatively small diameter of the accumulation mode and large diameter of the coarse mode. In addition, mean single scattering albedo values were relatively high (0.93 $\pm$ 0.02) perhaps indicating a difference in the mass absorption efficiencies of an aerosol whose primary absorbing component is dust and not BC. When low-level flow from Arabia was accompanied by upper-level flow from the Indian subcontinent, mean aerosol optical depths increased from 0.19 to 0.38. In addition, marine boundary layer BC concentrations increased by a factor of 3, and single scattering albedo decreased to 0.89 $\pm$ 0.02 presumably due to subsidence of upper troposphere air into the boundary layer.

[111] Transport of low-level air from the Indian subcontinent resulted in the highest concentrations of nss sulfate, POM, BC, and IOM measured during the experiment. Of these air masses, transport from the eastern Indian subcontinent near Calcutta resulted in the highest concentrations of each of these chemical components. Sulfate aerosol and a burning component composed of BC, KNO_3, and K_2NO_3 dominated both the sub-1 μm and sub-10 μm extinction.

[112] The contribution of sea salt to sub-10 μm extinction for the INDOEX continentally influence regions ranged from 7% for the eastern Indian subcontinent to 44% for air masses from Arabia. These values are lower than those reported for the Pacific and Atlantic Oceans, indicating the importance of non-sea-salt chemical components in determining the aerosol radiative forcing in the heavily impacted regions of the Indian Ocean.

[113] The *Ronald H. Brown* component of the 1999 INDOEX IFP had the instrumentation required for characterizing both surface and column aerosol properties relevant to radiative forcing. Improvements could be made, however, to achieve more accurate estimates of extinction due to each chemical component. These include (1) measuring the size distribution and determining the molecular composition of IOM and (2) determining the chemical composition of the aerosol organic matter. The latter would help in determining the hygroscopicity of the organic aerosol and the origin of the organic species in the sub- and supermicron size ranges. Despite these shortcomings, the regional aerosol properties presented here provide a unique data set for comparison to parameters derived from chemical transport and radiative transfer models and satellite retrievals.

[114] **Acknowledgments.** We thank Drew Hamilton for logistical assistance and the officers and crew of the NOAA Research Vessel *Ronald H. Brown*. This research was funded by the Aerosol Project of the NOAA Climate and Global Change Program and the Global Aerosol Climatology Project of the NASA Earth System Science Program. This is NOAA PMEL contribution 2256 and JISAO contribution 786.

References

Anderson, T. L., and J. A. Ogren, Determining aerosol radiative properties using the TSI 3563 integrating nephelometer, *Aerosol. Sci. Technol.*, *29,* 57–69, 1998.

Anderson, T. L., D. S. Covert, J. D. Wheeler, J. M. Harris, K. D. Perry,

B. E. Trost, D. J. Jaffe, and J. A. Ogren, Aerosol backscatter fraction and single scattering albedo: Measured values and uncertainties at a coastal station in the Pacific Northwest, *J. Geophys. Res*., *104*, 26,793–26,807, 1999.

Andreae, M. O., W. Elbert, and S. J. de Mora, Biogenic sulfur emissions and aerosols over the tropical South Atlantic, 3, Atmospheric dimethylsulfide, aerosols, and cloud condensation nuclei, *J. Geophys. Res*., *100*, 11,335–11,356, 1995.

Ansari, A. S., and S. N. Pandis, Water absorption by secondary organic aerosol and its effect on inorganic aerosol behavior, *Environ. Sci. Technol*., *34*, 71–77, 2000.

Ayers, G. P., M. D. Keywood, and J. L. Gras, TEOM vs. manual gravimetric methods for determination of PM2.5 aerosol mass concentrations, *Atmos. Environ*., *33*, 3717–3721, 1999.

Bates, T. S., P. K. Quinn, D. J. Coffman, J. E. Johnson, T. L. Miller, D. S. Covert, A. Wiedensohler, S. Leinert, A. Nowak, and C. Neususess, Regional physical and chemical properties of the marine boundary layer aerosol across the Atlantic during Aerosols99: An overview, *J. Geophys. Res*., *106*, 20,767–20,782, 2001.

Berner, A., C. Lurzer, F. Pohl, O. Preining, and P. Wagner, The size distribution of the urban aerosol in Vienna, *Sci. Total Environ*., *13*, 245–261, 1979.

Bond, T. C., T. L. Anderson, and D. Campbell. Calibration and intercomparison of filter-based measurements of visible light absorption by aerosols. *Aerosol Sci. Technol*., *30*, 582–600, 1999.

Bray, W. H., Water vapor pressure control with aqueous solutions of sulfuric acid, *J. Mater*., *5*, 233–248, 1970.

Bromley, L. A., Thermodynamic properties of strong electrolytes in aqueous solutions, *AIChE J., 19*, 313–320, 1973.

Cachier, H., C. Liousse, P. Buat-Menard, and A. Gaudichet, Particulate content of savanna fire emissions, *J. Atmos. Chem*., *22*, 123–148, 1995.

Cahill, T. A., R. A. Eldred, and P. J. Feeney, Particulate monitoring and data analysis for the National Park Service, 1982–1985, Univ. of Calif., Davis, 1986.

Charlson, R. J., T. L. Anderson, and H. Rodhe, Direct climate forcing by anthropogenic aerosols: Quantifying the link between atmospheric sulfate and radiation, *Contrib. Atmos. Phys*., 72(1), 79–94, 1999.

Chiapello, I., G. Bergametti, B. Chatenet, F. Dulac, I. Jankowiak, C. Liousse, and E. S. Soares, Contribution of the different aerosol species to the aerosol mass load and optical depth over the northeastern tropical Atlantic, *J. Geophys. Res*., *104*, 4025–4035, 1999.

Clarke, A. D., S. Howell, P. K. Quinn, T. S. Bates, J. A. Ogren, E. Andrews, A. Jefferson, and A. Massling, The INDOEX aerosol: A comparison and summary of chemical, microphysical, and optical properties observed from land, ship, and aircraft, *J. Geophys. Res*., *107*(DX), 10.1029/2001JD000572, in press, 2002.

Clegg, S. L., and P. Brimblecombe, Potential degassing of hydrogen chloride from acidified sodium chloride droplets, *Atmos. Environ*., *19*, 465–470, 1985.

Cohen, M. D., R. C. Flagan, and J. H. Seinfeld, Studies of concentrated electrolyte solutions using the electrodynamic balance, 1, Water activities for single-electrolyte solutions, *J. Phys. Chem*., *91*, 4563–4574, 1987.

Covert, D. S., A. Wiedensohler, and L. M. Russell, Particle charging and transmission efficiencies of aerosol charge neutralizers, *Aerosol Sci. Technol*., *27*, 208–214, 1997.

Dick, W. D., P. Saxena, and P. H. McMurry, Estimation of water uptake by organic compounds in submicron aerosols measured during the Southeastern Aerosols and Visibility Study, *J. Geophys. Res*., *105*, 1471–1479, 2000.

Draxler, R. R., Hybrid Single-Particle Lagrangian Integrated Trajectories (HY-SPLIT): Version 3.0. user's guide and model description, *Tech. Rep. ERLARL-195*, Natl. Oceanic and Atmos. Admin. Silver Spring, Md., 1992.

Feely, R. A., G. J. Massoth, and G. T. Lebon, Sampling of marine particulate matter and analysis by X-ray fluorescence spectrometry, In Hurd, D. C., Spencer, D. W. (eds.), *Marine Particles: Analysis and Characterization, Geophys. Monogr. Ser.*, vol. 63, edited by D. C. Hurd and D. W. Spencer, pp. 251–257, AGU, Washington, D. C., 1991.

Feely, R. A., E. T. Baker, G. T. Lebon, J. F. Gendron, G. J. Massoth, and C. W. Mordy, Chemical variations of hydrothermal particles in the 1996 Gorda Ridge Event and chronic plumes, *Deep Sea Res*., *45*, 2637–2664, 1998.

Ferek, R. J., J. S. Reid, P. V. Hobbs, D. R. Blake, and C. Liousse, Emission factors of hydrocarbons, halocarbons, trace gases, and particles from biomass burning in Brazil, *J. Geophys. Res*., *103*, 32,107–32,118, 1998.

Hegg, D. A., J. Livingston, P. V. Hobbs, T. Novakov, and P. Russell, Chemical apportionment of aerosol column optical depth off the mid-Atlantic coast of the United States, *J. Geophys. Res*., *102*, 25,293–25,303, 1997.

Holland, H. D., *The Chemistry of the Atmosphere and Oceans*, p. 154, John Wiley, New York, 1978.

Kasten, F., and A. T. Young, Revised optical air mass tables and approximation formula, *Appl. Opt*., *28*, 4735–4738, 1989.

Langner, J., and H. Rodhe, A global three-dimensional model of the tropospheric sulfur cycle, *J. Atmos. Chem*., *13*, 225–263, 1991.

Li, X., D. Savoie, K. Voss, and J. M. Prospero, Dominance of mineral dust in aerosol light-scattering in the North Atlantic trade winds, *Nature, 380*, 416–419, 1996.

Liousse, C., J. E. Penner, C. Chuang, J. J. Walton, and H. Eddleman, A global three-dimensional study of carbonaceous aerosol, *J. Geophys. Res*., *101*, 19,411–19,432, 1996.

Liu, X., P. Van Espen, F. Adams, J. Cafmeyer, and W. Maenhaut, Biomass burning in Southern Africa: Individual particle characterization of atmospheric aerosols and savanna fire samples, *J. Atmos. Chem*., *36*, 135–155, 2000.

Malm, W. C., J. F. Sisler, D. Huffman, R. A. Eldred, and T. A. Cahill, Spatial and seasonal trends in particle concentration and optical extinction in the United States, *J. Geophys. Res*., *99*, 1347–1370, 1994.

McInnes, L. M., P. K. Quinn, D. S. Covert, and T. L. Anderson, Gravimetric analysis, ionic composition, and associated water mass of the marine aerosol, *Atmos. Environ*., *30*, 869–884, 1996.

McInnes, L. M., M. Bergin, J. Ogren, and S. Schwartz, Apportionment of light scattering and hygroscopic growth to aerosol composition, *Geophys. Res. Lett*., *25*, 513–516, 1998.

Meyer, M., J. Lijek, and D. Ono, Continuous PM10 measurements in a woodsmoke environment, PM10 standards and nontraditional particulate source controls, edited by J. C. Chow and D. M. Ono, vol. 1, *Tech. Rep. TR-22*, pp. 24–38, Air and Waste Manage. Assoc., Pittsburgh, Pa., 1992.

Neususess, C., D. Weise, W. Birmili, H. Wex, A. Wiedensohler, and D. S. Covert, Size-segregated chemical, gravimetric and number distribution-derived mass closure of the aerosol in Sagres, Portugal during ACE-2, *Tellus, 52*, 169–184, 2000.

Neususess, C., A. Massling, and J. Heintzenberg, Carbonaceous aerosol over the Indian Ocean: OC/EC fractions and speciations from size-segregated samples taken on board the R/V *Ron Brown, J. Geophys. Res*., *107*(DX), 10.1029/2001JD000327, in press, 2002.

Novakov, T., D. A. Hegg, and P. V. Hobbs, Airborne measurements of carbonaceous aerosols on the East Coast of the United States, *J. Geophys. Res*., *102*, 30,023–30,030, 1997.

Novakov, T., T. S. Bates, and P. K. Quinn, Shipboard measurements of concentrations and properties of carbonaceous aerosols during ACE-2, *Tellus, Ser. B.*, *52*, 228–238, 2000.

Novakov, T., and V. Ramanathan, Origin of carbonaceous aerosol over the tropical Indian Ocean: Biomass or fossil P, *Geophys. Res. Lett*., *27*, 4061–4064, 2001.

Patterson, E. M., and C. K. McMahon, Absorption characteristics of forest fire particulate matter, *Atmos. Environ*., *18*, 2541–2551, 1984.

Penndorf, R., Tables of refractive index for standard air and the Rayleigh scattering coefficient for the spectral region between 0.2 and 20 μm and their application to atmospheric optics, *J. Opt. Soc. Am*., *47*, 176–182, 1957.

Perry, K. D., T. A. Cahill, R. A. Eldred, D. D. Dutcher, and T. E. Gill, Long-range transport of North African dust to the eastern United States, *J. Geophys. Res*., *102*, 11,225–11,238, 1997.

Pilinis, C., and J. H. Seinfeld, Continued development of a general equilibrium model for inorganic multicomponent atmospheric aerosols, *Atmos Environ*., *21*, 2453–2466, 1987.

Pitzer, K. S., and G. Mayorga, Thermodynamics of electrolytes, II, Activity and osmotic coefficients for strong electrolytes with one or both ions univalent, *J. Phys. Chem*., *77*, 2300–2308, 1973.

Quinn, P. K., and D. J. Coffman, Local closure during ACE 1: Aerosol mass concentration and scattering and backscattering coefficients, *J. Geophys. Res*., *103*, 16,575–16,596, 1998.

Quinn, P. K., V. N. Kapustin, T. S. Bates, and D. S. Covert, Chemical and optical properties of marine boundary layer aerosol particles of

the mid-Pacific in relation to sources and meteorological transport, *J. Geophys. Res*., *101*, 6931–6951, 1996.

Quinn, P. K., D. J. Coffman, V. N. Kapustin, T. S. Bates, and D. S. Covert, Aerosol optical properties in the marine boundary layer during ACE 1 and the underlying chemical and physical aerosol properties, *J. Geophys. Res*., *103*, 16,547–16,563, 1998.

Quinn, P. K., et al., Surface submicron aerosol chemical composition: What fraction is not sulfate?, *J. Geophys. Res*., *105*, 6785–6806, 2000a.

Quinn, P. K., T. S. Bates, D. J. Coffman, T. L. Miller, J. E. Johnson, D. S. Covert, J. P. Putaud, C. Nesusseus, and T. Novakov, A comparison of aerosol chemical and optical properties from the first and second aerosol characterization experiments, *Tellus, Ser. B, 52*, 239–257, 2000b.

Quinn, P. K., D. J. Coffman, T. S. Bates, T. L. Miller, J. E. Johnson, K. Voss, E. J. Welton, and C. Neusüss, Dominant Aerosol Chemical Components and Their Contribution to Extinction During the Aerosols99 Cruise Across the Atlantic. *J. Geophys. Res*., *106*(D18), 20,783–20,810, 2001.

Ramanathan, V., et al., Indian Ocean Experiment: An integrated analysis of the climate forcing and effects of the great Indo-Asian haze *J. Geophys. Res*., *106*(D22), 28, 371–28,398, 2001.

Reynolds, R. M., M. A. Miller, and M. J. Bartholomew, Design, operation, and calibration of a shipboard fast-rotating shadowband radiometer, *J. Atmos. Oceanic Technol., 18*, 200–214, 2001.

Robinson, R. A., and R. H. Stokes, *Electrolyte Solutions*, 2nd ed., Butterworths, London, 1965.

Satheesh, S. K., V. Ramanathan, X. L. Jones, J. M. Lobert, I. A. Podgorny, J. M. Prospero, B. N. Holben, and N. G. Loeb, A model for the natural and anthropogenic aerosols over the tropical Indian Ocean derived from the Indian Ocean Experiment data, *J. Geophys. Res*., *104*, 27,421–27,440, 1999.

Savoie, D. L., and J. M. Prospero, Water-soluble potassium, calcium, and magnesium in the aerosols over the tropical North Atlantic, *J. Geophys. Res*., *85*, 385–392, 1980.

Saxena, P., L. M. Hildemann, P. H. McMurry, and J. H. Seinfeld, Organics alter hygroscopic behavior of atmospheric particles, *J. Geophys. Res*., *100*, 18,755–18,770, 1995.

Seinfeld, J. H., *Atmospheric Chemistry and Physics of Air Pollution*, p. 296, John Wiley, New York, 1986.

Seinfeld, J. H., and S. N. Pandis, *Atmospheric Chemistry and Physics*, John Wiley, New York, 1998.

Shaw, G. E., Sun photometry, *Bull. Am. Meteorol Soc*., *64*, 4–9, 1983.

Sheridan, P., A. Jefferson, and J. Ogren, Spatial variability of aerosol radiative properties over the Indian Ocean during INDOEX, *J. Geophys. Res*., *107*(DX), 10.1029/2000JD000166, in press, 2002.

Sokolik, I. N., and O. B. Toon, Incorporation of mineralogical composition into models of the radiative properties of mineral aerosol from UV to IR wavelengths, *J. Geophys. Res*., *104*, 9423–9444, 1999.

Stelson, A. W., Urban aerosol refractive index prediction by partial molar refraction approach, *Environ. Sci. Technol*., *24*, 1676–1679, 1990.

Stratman, F., and A. Wiedensohler, A new data inversion algorithm for DMPS measurements, *J. Aerosol Sci*., *27*, 339–340, 1997.

Tang, I. N., Chemical and size effects of hygroscopic aerosols on light scattering coefficients, *J. Geophys. Res*., *101*, 19,245–19,250, 1996.

Tang, I. N., and H. R. Munkelwitz, Simultaneous determination of refractive index and density of an evaporating aqueous solution droplet, *Aerosol. Sci. Technol*., *15*, 201–207, 1991.

Tang, I. N., and H. R. Munkelwitz, Water activities, densities, and refractive indices of aqueous sulfates and sodium nitrate droplets of atmospheric importance, *J. Geophys. Res*., *99*, 18,801–18,808, 1994.

Tang, I. N., A. C. Tridico, and K. H. Fung, Thermodynamic and optical properties of sea-salt aerosol, *J. Geophys. Res*., *102*, 23,269–23,275, 1997.

Tangren, C. D., Scattering coefficient and particulate matter concentration in forest fire smoke, *J. Air Pollut. Control Assoc*., *32*, 729–732, 1982.

Turpin, B. J., and H. Lim, Species contribution to PM2.5 concentrations: Revisiting common assumptions for estimating organic mass, *Aerosol. Sci. Technol*., *35*, 602–610, 2001.

Turpin, B. J., J. J. Huntzicker, and S. V. Hering, Investigation of organic aerosol sampling artifacts in the Los Angeles Base, *Atmos. Environ*., *28*, 23,061–23,071, 1994.

Turpin, B. J., P. Saxena, and E. Andrews, Measuring and simulating particulate organics in the atmosphere: Problems and prospects, *Atmos. Environ*., *34*, 2983–3013, 2000.

Welton, E. J., K. J. Voss, P. K. Quinn, J. R. Campbell, J. D. Spinhirne, H. R. Gordon, and J. Johnson, Measurements of aerosol vertical profiles and optical properties during INDOEX 1999 using micropulse lidars, *J. Geophys. Res*., *107*(DX), 10.1029/2000JD000038, in press, 2002.

Wiedensohler, A., et al., Intercomparison study of the size-dependent counting efficiency of 26 condensation particle counters, *Aerosol Sci. Technol*., *27*, 224–254, 1997.

Zdanovskii, A. B., *Tr. Solyanoi Lab. Vses. Inst. Galurgii Akad. Nauk SSSR*, no. 6, 1936.

T. S. Bates, D. J. Coffman, J. E. Johnson, T. L. Miller, and P. K. Quinn, Pacific Marine Environmental Laboratory, NOAA, Seattle, WA 98115, USA. (quinn@pmel.noaa.gov)

M. Miller, Environmental Sciences Department, Brookhaven National Laboratory, Upton, NY 11973, USA.

C. Neusüss, Institute for Tropospheric Research, 04318, Leipzig, Germany.

P. J. Sheridan, Climate Monitoring and Diagnostics Laboratory, NOAA, Boulder, CO 80303, USA.

E. J. Welton, Goddard Earth Science and Technology Center, University of Maryland, Baltimore County, Greenbelt, MD 20771, USA.)